2009

Inclusion modification in steel castings using automated inclusion analysis

Vintee Singh

Department:

INCLUSION MODIFICATION IN STEEL CASTINGS USING AUTOMATED INCLUSION ANALYSIS

by

VINTEE SINGH

A THESIS

Presented to the Faculty of the Graduate School of the

MISSOURI UNIVERSITY OF SCIENCE AND TECHNOLOGY

In Partial Fulfillment of the Requirements for the Degree

MASTER OF SCIENCE IN MATERIALS SCIENCE AND ENGINEERING

2009

Approved by

Kent D. Peaslee, Advisor

Von L. Richards

Simon Lekakh

ABSTRACT

The objective of this research is to study the effects of changing the melt and ladle practices (deoxidation, slag, refractory types, etc.) in steel foundries on the cleanliness and toughness of steel castings. This study used an automated inclusion analyzer ASPEX PICA-1020, which provides a rapid and accurate method for determining the composition, size, number, and spacing of the inclusions present in steel samples.

The first step in this research was to complete a series of industrial tests to benchmark the current foundry ladle practices with respect to cleanliness of the cast steel. Trials were conducted at steel foundries using induction and arc furnaces of capacity 1 to 20 tons. Samples collected from the furnace, ladle, and cast products were analyzed for inclusions, using ASPEX, and for their oxygen content, using a Leco analyzer.

The next step was to conduct industrial trials to study the effects of ladle metallurgy (Ca-treatment through wire injection, gas stirring, etc.) on inclusions and mechanical properties of the casting. Several 1000 lb ladles of steel were treated with different amounts and speeds of Ca and CaSi wire injection and argon stirring. The inclusions and the oxygen content were analyzed in the samples collected. Charpy impact tests were conducted on the cast products to observe the relationship between inclusions and the toughness of the cast steel. FLUENT modeling was done to understand the effects of various parameters of the ladle-practice on flotation of inclusions.

In all the heats conducted with Ca-additions in the ladle, the fraction of area covered by inclusions and the total oxygen was found to decrease after the Ca-treatment. The toughness of the castings were found to be indirectly proportional to the inclusions and increased with an increase in the amount of Ca-added in the ladle.

ACKNOWLEDGMENTS

I wish to express my deepest gratitude to my advisor, Dr. Kent D. Peaslee for providing me with an opportunity to pursue a master's degree in Missouri University of Science and Technology. His suggestions, guidance and personal attention have been a great motivational factor for me to complete this research.

I would like to thank my committee members, Dr. Von L. Richards and Dr. Simon Lekakh for their time and effort in reviewing my progress.

I acknowledge the support of U.S. Army Benet Labs for providing funding for this research. I would also like to thank the Steel Founders Society of America and the member companies that participated in this research.

I thank Tim Drake from Aspex Corporation for helping with the operation of the Aspex equipment throughout this research.

Finally, I would like to thank my lab mates William Peach, Meghan McGrath, Angella Schulte, Jared Teague, Dan Snyder, Darryl Kline and Phani Angara for their continuous support.

TABLE OF CONTENTS

LIST OF ILLUSTRATIONS

LIST OF TABLES

1. LITERATURE SURVEY

An increase in demand for higher quality steel is forcing steelmakers to ensure that their steel products meet more stringent ‘‘cleanliness’’ requirements. Nonmetallic inclusions are a significant problem in cast steels because they may lead to problems in castings that require expensive casting repairs or result in failures while in use. The mechanical properties for steel are affected by the volume fraction, size, distribution, composition, and morphology of inclusions. The toughness of steel is very important in many critical applications where fracture resulting in failure could produce catastrophic effects. Hence, the exact determination of non-metallic inclusions is essential to the success of research aimed at increasing toughness of steel parts.

1.1. SOURCE OF INCLUSIONS IN STEEL CASTINGS

Most of the inclusions in steel are the product of the deoxidation process. The aim of deoxidation or “killing” is to reduce the dissolved oxygen content of the steel. As the steel solidifies, oxygen dissolved in the liquid cannot be accommodated by the solid crystal structure and therefore reacts with dissolved carbon forming CO gas which is trapped in the casting as porosity or pinholes. The addition of deoxidizers to molten steel reduces the dissolved oxygen in the system through the formation of liquid or solid oxide phases. When the steel starts to cool, there is a corresponding decrease in oxygen solubility and inclusions precipitate to satisfy the new and constantly changing equilibrium conditions. The inclusions which precipitate early in the cooling process have a greater opportunity to escape through flotation. However, as the metal solidifies and dendrites continue to grow larger, the inclusions precipitated late during solidification become entrapped, and appear as small non-metallic phases in the finished product [1].

Elements used for deoxidation are those that have a greater affinity for oxygen than carbon and form thermodynamically more stable oxides than iron oxide. These elements include aluminum, silicon, manganese, calcium, zirconium, titanium, magnesium, boron and rare earth metals (REM). Figure 1.1 summarizes the deoxidation effects of several common deoxidizers.

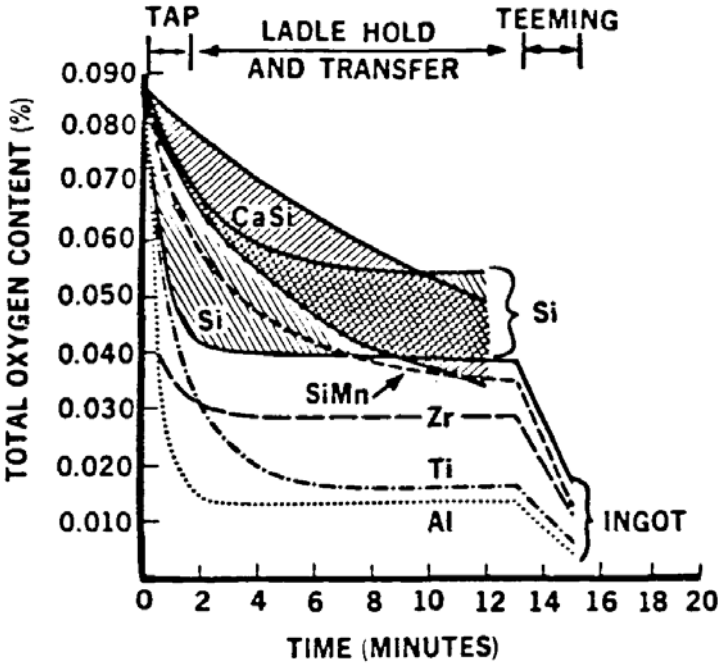

Figure 1.1. Deoxidation results of the common deoxidizers [2]

The most common deoxidizer for steel castings is aluminum, which produces solid particles of Al_2O_3. The coalescence of these particles forms agglomerates of irregular shape called 'alumina clusters'. The clusters significantly affect the mechanical and fatigue properties of steel, and may also result in the generation of surface defects [3]. Alumina inclusions are dendritic when formed in a high oxygen environment and often form clusters as a of the collision of smaller particles, as shown in Figure 1.2(a,b) [4].

Exogenous inclusions arise from unintended chemical and mechanical interaction of liquid steel with its surroundings. They generally have the most deleterious effect on mechanical properties because of their large size and location near the surface [5]. The majority of these inclusions are formed by reoxidation in which liquid steel, having "free" deoxidants (Al, Mn or Ca) dissolved in the molten steel, picks up oxygen from contact with the air during pouring and transportation through the gating system. In addition, inclusions can be formed by reaction of the liquid steel with water vaporizing from the molding sands and debris in the gating system. The exogenous inclusions in steel are sporadic because they are usually entrapped accidentally during tapping, pouring and

solidification. These inclusions act as heterogeneous nucleation sites for precipitation of new inclusions during their motion in molten steel [6].

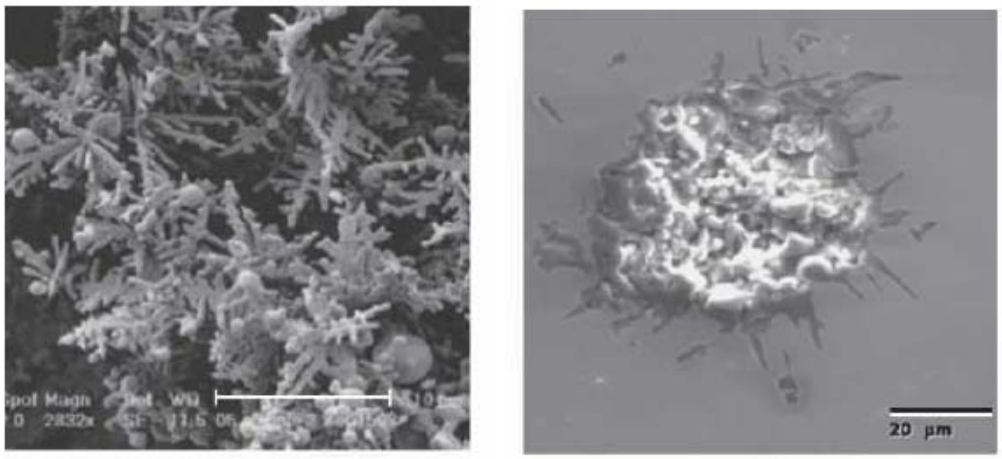

a) b)

Figure 1.2. Morphology of alumina inclusions generated during deoxidation of low carbon Al-killed steels a) dendritic alumina and b) alumina cluster [4]

Figure 1.3 explains the formation of inclusions by both the deoxidation and reoxidation mechanisms, in a fully killed molten steel deoxidized with silicon and manganese, containing more than 0.01 wt. % of aluminum. The deoxidation mechanism is explained on the left side of the figure. The top bar represents the amount of oxygen remaining in solution in the liquid steel after deoxidation, while the remaining bars indicate the large amount of aluminum, along with the silicon and manganese present. As the steel starts to cool, aluminum, being a stronger deoxidizer than silicon and manganese, combines with oxygen to form alumina inclusions. The availability of oxygen is limited in this reaction mechanism and once the oxygen is reduced to very low levels, the reaction ceases. When more than 0.01 % Al is at equilibrium with the steel, the amount of oxygen is reduced to very low levels by reacting with the aluminum to form alumina during cooling and solidification, resulting in no Mn or Si present in the indigenous inclusions. However, as shown in the reoxidation mechanism in the figure, the large oxygen supply first reacts with aluminum in the steel through the formation of

alumina. If sufficient aluminum is present to deoxidize the steel and/or exposure time is insufficient, then only alumina will form as the reoxidation product. But if Al is less than 0.01 wt. %, and/or the exposure is quite severe, then the aluminum deoxidation will be followed by Si and Mn. In such a case, the formation of deoxidation products appears to take place in stages. First alumina inclusions are formed, followed by formation of complex alumina-manganese-silicates. If the reaction is too severe, iron oxide formation can also take place [1].

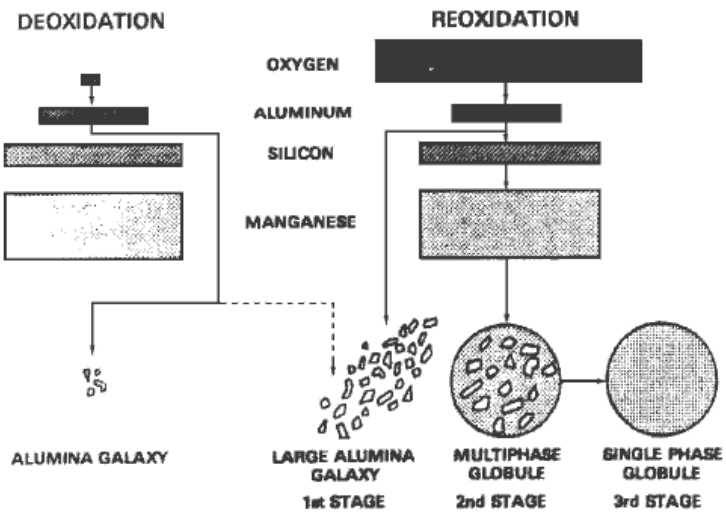

Figure 1.3. Graphical representation of formation of inclusions in as-cast steel deoxidized with aluminum, with more than 0.01 % Al retained in the steel [1]

1.2. EFFECTS OF INCLUSIONS ON MECHANICAL PROPERTIES

The ultimate purpose of this work is to obtain steel casting with improved mechanical properties through improved micro-cleanliness. Though the presence of inclusions can never be entirely avoided, the quantity, size, shape, distribution and composition can be modified to achieve better mechanical properties.

In cast steel, non-metallic inclusions are one of the primary sites at which void nucleation occurs. Voids are nucleated at one of these second-phase particles, either by decohesion of the particle-matrix interface or by particle fracture. The voids nucleated at the particle sites grow until they coalesce by impingement or by the process of void sheet

coalescence [7]. Void sheet coalescence requires fracture of the ligament between the voids created at the larger non-metallic inclusions. Figure 1.4 shows the fracture of steel due to the growth and coalescence of voids nucleated at some of the inclusions.

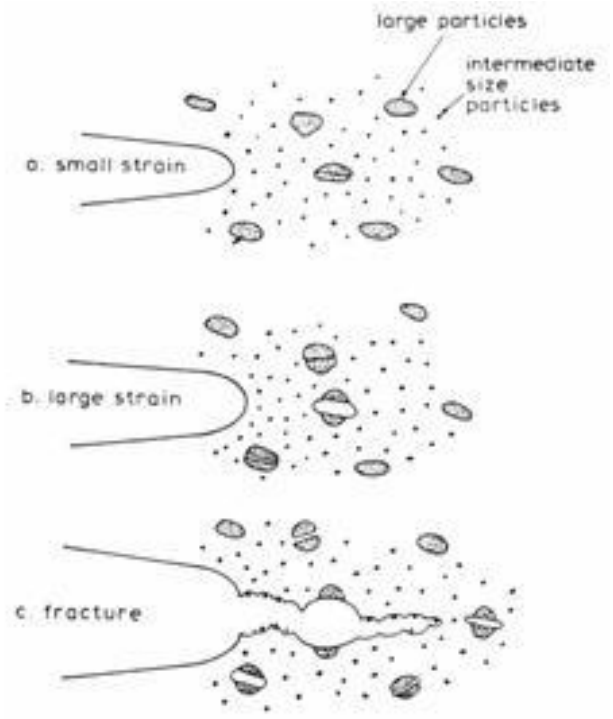

Figure 1.4. Nucleation of voids on inclusions in (a) and b), and (c) fracture of steel [7]

The ability of a material to arrest an existing crack and prevent the onset of rapid crack propagation at stress levels below the yield stress is called fracture toughness [8]. The characteristic inclusion volume fraction and the inclusion spacing have been shown to greatly influence the fracture toughness of steel. Recent research has shown that decreasing the volume fraction of inclusions that induce void nucleation and increasing the inclusion spacing result in significant improvement in toughness [9]. Hahn *et al* [10] found that fracture toughness of steel (K_{1C}) inversely varied with the volume fraction of the inclusions according to the equation:

$$K_I = V_f^{-\frac{1}{6}} \sqrt{2\left(\frac{\pi}{6}\right)^{\frac{1}{3}} \sigma_{yield} Ed} \quad (1)$$

where, K_1 = fracture toughness, V_f = volume fraction of the inclusions, σ_{yield} = yield strength, E= Young's modulus, and d= particle diameter. The fracture toughness varies directly with the inclusion spacing according to the equation:

$$K_1 = (2\sigma_{yield} Es)^{1/2} \quad (2)$$

where, K_1 = fracture toughness, σ_{yield} = yield strength, E= Young's modulus, and s= average spacing between the inclusions

Apart from the toughness, inclusions have been reported to be detrimental to other physical properties of steels too. The machinability of steel is impaired by oxide inclusions which never deform plastically at any temperature less than or equal the highest possible temperature in the flow zone of the steel; that is those which have an index of deformability near zero at all such temperatures. Important inclusions in this category are corundum, escolaite, spinels and calcium-aluminates [11]. Large exogenous inclusions also cause inferior surface appearance, poor polishability, reduced resistance to corrosion, and, in severe cases, slag lines and laminations [12]. Inclusions adversely affect the weldability of cast steel, causing laminations in the unmelted heat-affected zone, burning and hot-tearing from sulfides, and crack formation from oxides [13].

1.3. CALCIUM TREATMENT

1.3.1. Effects of Ca-treatment on Inclusions. Al_2O_3 inclusions form clusters, which significantly harm the mechanical and fatigue properties of steel. One technique used to diminish the harmful effects of Al_2O_3 inclusions in steel is calcium treatment. During Ca-treatment, the alumina inclusions are converted to molten calcium aluminates which are globular in shape. The calcium aluminate inclusions retained in the steel suppress the formation of harmful MnS stringers during solidification of steel .Ca-

treatment also helps in modifying MnS inclusions to spherical CaS inclusions. This change in inclusion composition and shape due to Ca-treatment is known as inclusion morphology control. This is demonstrated schematically in Figure 1.5.

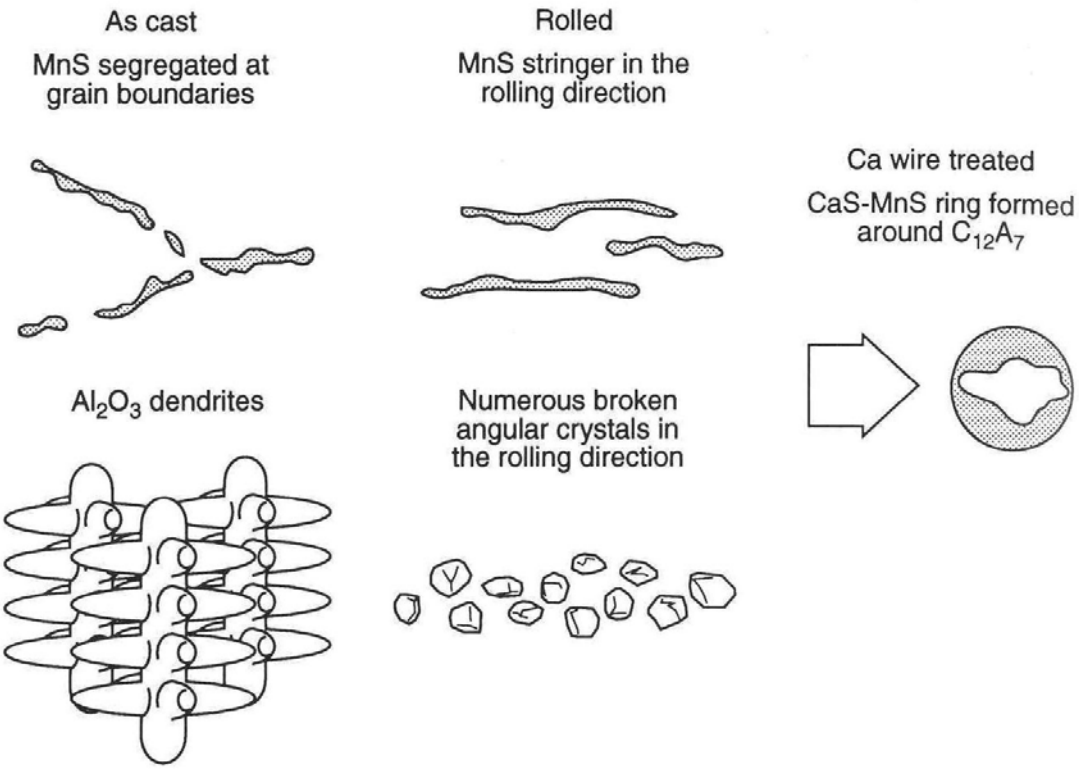

Figure 1.5. Schematic illustration of formation of calcium aluminates and suppression of formation of MnS inclusions with Ca-treatment of steel [14]

When alumina is modified to calcium aluminate, the reaction sequence followed is: Al_2O_3 -> CA_6 -> CA_2 -> CA -> $C_{12}A_7$, where C and A denotes CaO and Al_2O_3, respectively [15]. The CaO- Al_2O_3 phase diagram in Figure 1.6 shows the presence of liquid calcium aluminates, CA_2, CA, $C_{12}A_7$ at steelmaking temperatures (~ 1600 ^oC) which means that unlike solid alumina inclusions, these liquid inclusions are easier to float to the surface. Also, they do not stick to and block ladle and tundish nozzles and solidification fronts during pouring and casting, which is a major issue in continuous casting of steel [16].

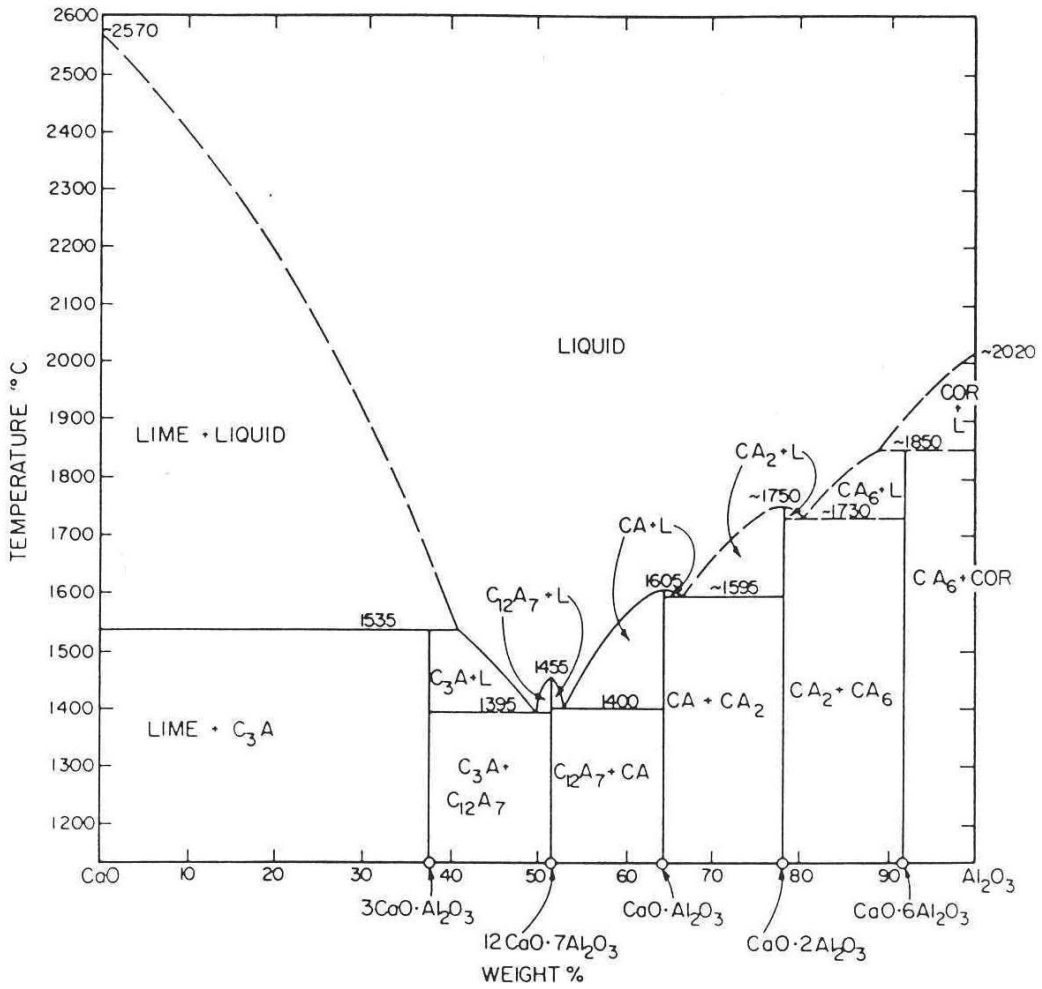

Figure 1.6. CaO- Al_2O_3 binary phase diagram [14]

As reactions progress to form calcium aluminates richer in calcium, the activity of the Al_2O_3 decreases, allowing more of the Al to react with oxygen, providing even better deoxidation. Plant data in Figure 1.7 shows that, the deoxidation of steel with aluminum is shifted to lower levels of residual dissolved oxygen upon subsequent calcium treatment because of the lower alumina activity in the modified inclusions [17].

In steels not treated with calcium, the sulfur precipitates as finely dispersed MnS particles in the interdendritic liquid that freezes last. The MnS delineate the prior austenitic grain boundaries in the as-cast structure. During hot rolling, the MnS particles are deformed, resulting in stringers in the rolled product. These stringers make the final product brittle and susceptible to cracking [11].

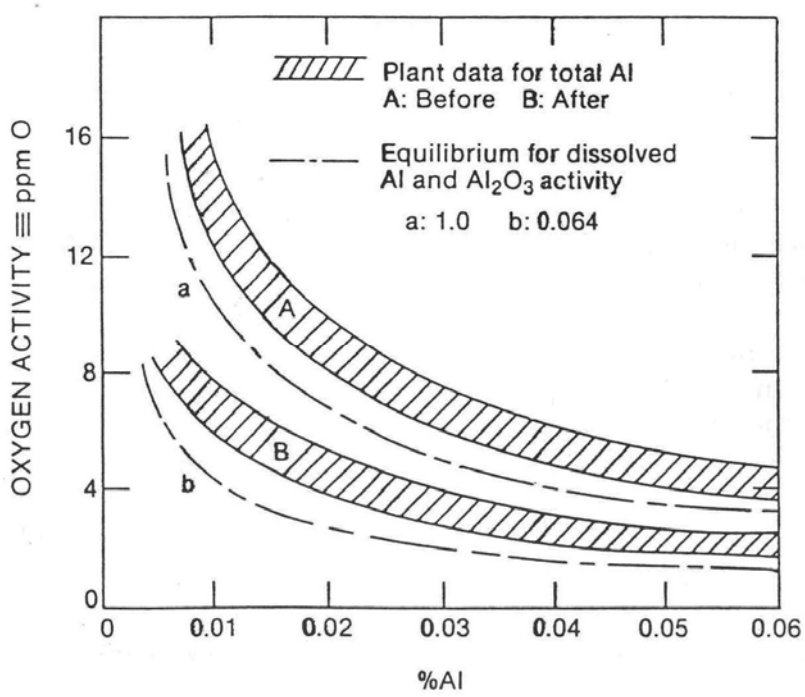

Figure 1.7. Oxygen sensor readings before and after CaSi injection into Al-killed steel at 1600 +/- 15 ^{o}C [17]

In calcium-treated low sulfur steels, the grain boundary precipitation of MnS during solidification is suppressed as a result of the precipitation of sulfur as a Ca(Mn)S complex on the calcium aluminate inclusions by the following reaction[18]:

$$(CaO) + 2/3[Al] + 2[S] + [Mn] = (CaS{\cdot}MnS) + 1/3\ (Al_2O_3) \qquad (3)$$

The extent of sulfide shape control that can be achieved during solidification of calcium-treated steel depends on the total oxygen, sulfur and calcium contents of the steel. In steels with relatively high sulfur contents, e.g. > 100 ppm, sulfide shape control by means of calcium treatment is not feasible. To minimize the occurrence of sulfide stringers in such steels, the addition of Te or Se has been found to be beneficial [19].

1.3.2. Thermodynamics of Calcium Addition. When calcium is added, the following series of reactions are expected to occur to a varying extent in Al-killed steels containing alumina inclusions.

$$Ca\ (l) = Ca\ (g) \quad (4)$$

$$Ca\ (g) = [Ca] \quad (5)$$

$$[Ca] + [O] = CaO \quad (6)$$

$$[Ca] + [S] = CaS \quad (7)$$

$$[Ca] + (x+1/3)[\ Al_2O_3] = CaO{\cdot}x\ Al_2O_3 + 2/3\ [Al] \quad (8)$$

$$CaO + 2/3[Al] + [S] = (CaS) + 1/3\ (Al_2O_3) \quad (9)$$

If the sulfur content of the steel is above a certain limit, calcium aluminate formation will be suppressed by CaS formation. The basic problem encountered in thermodynamic modeling of Ca-modification of inclusions is that there are too many variables to be considered in a two-dimensional description. A simple model was proposed by assuming most of the variables constant with only two variables and one parameter allowed to vary. *Holappa et. al* proposed a model for Ca-additions based on this same technique. They performed calculations for a steel grade with the chemistry: 0.35% C, 0.25% Si, and 0.50% Mn. Oxygen content was assumed to be constant at 20 ppm and the temperature at 1550 ^{o}C and sulfur was the variable parameter [20, 21]. Figure 1.8 illustrates the limits of the liquid area by calculating the saturation lines of solid calcium aluminates ($CaO{\cdot}Al_2O_3$, $CaO{\cdot}2Al_2O_3$) and CaS, respectively. The figure clearly shows how the growth of sulfur content increases the stability of CaS and thus contracts the liquid area.

In practical steelmaking, the scatter in the oxygen content before the calcium treatment and the unpredictable yield of calcium in solution to react with Al_2O_3 makes the calculation of optimum amount of Ca-addition difficult. So for the trials conducted in this study, the amounts of Ca-addition were varied over a wide range, in order to experimentally determine the values of calcium addition resulting in better inclusion modification and reduction.

1.3.3 Method of Ca-addition. The boiling point of calcium is 1491^{o}C (2716^{o}F) at atmospheric pressure, so it is in vapor state at steelmaking temperatures. Thus, when adding calcium to liquid steel, special measures must be taken to ensure its proper recovery in the steel bath. The injection of calcium below the surface of the steel through wire injection is a more effective method of Ca- addition than bulk addition, as it

suppresses Ca boiling because of the higher ferrostatic pressure. When Ca is injected at a depth, it is under a large external pressure, which increases its boiling point. Figure 1.9 shows the effect of external pressure on the boiling point of liquid calcium.

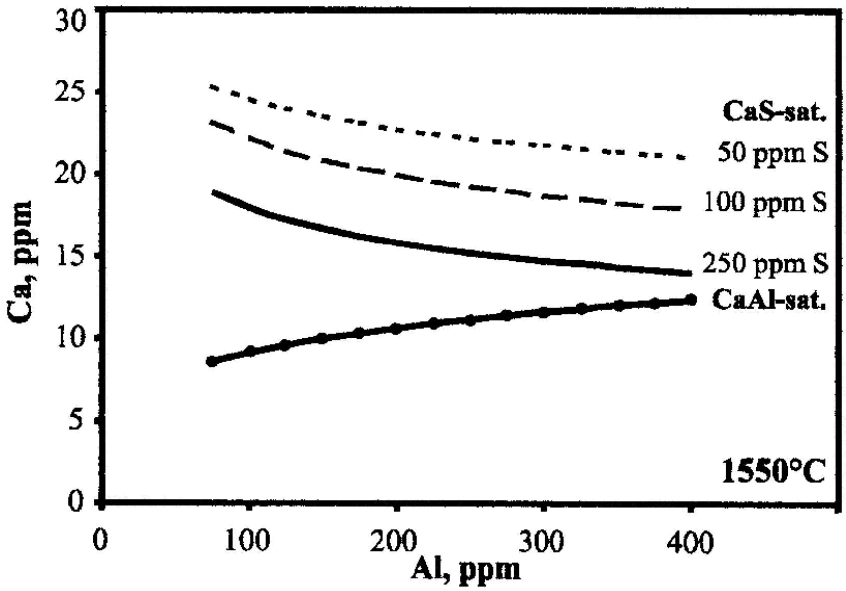

Figure 1.8. Saturation lines for calcium aluminates and CaS and liquid windows at different S levels at 1550^{o}C [21]

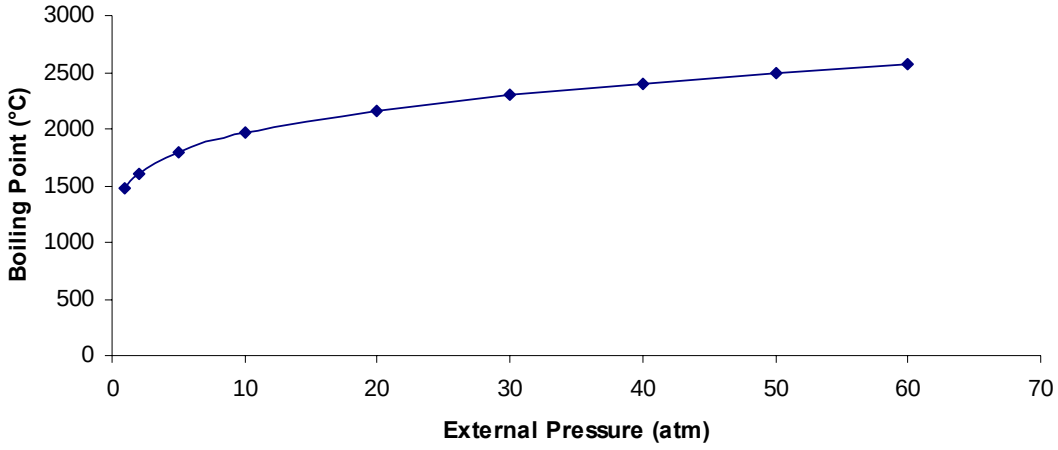

Figure 1.9. Effect of external pressure on the boiling point of liquid Ca [22]

The vapor pressure of liquid Ca is related to temperature by the following equation:

$$\log P = 9.67 - \frac{8190}{T} \quad [22] \tag{10}$$

where, P is external pressure and T is temperature.

At the boiling point of a liquid, the vapor pressure is equal to the external pressure, so if the external pressure is known, the boiling point of the liquid can be calculated. Also, at different depths in liquid steel the external pressure is equal to the pressure head given by:

$$P = \rho g h \tag{11}$$

where, ρ= density of steel, g = gravity, and h= depth in liquid

Assuming the ρ for steel as 7230 kg/m^3 [23], the variation of the boiling point of calcium with the depth of the wire in liquid steel is shown in Figure 1.10. This illustrates that a deeper injection in the ladle suppresses the boiling of calcium more, hence, giving a better reaction with the liquid steel.

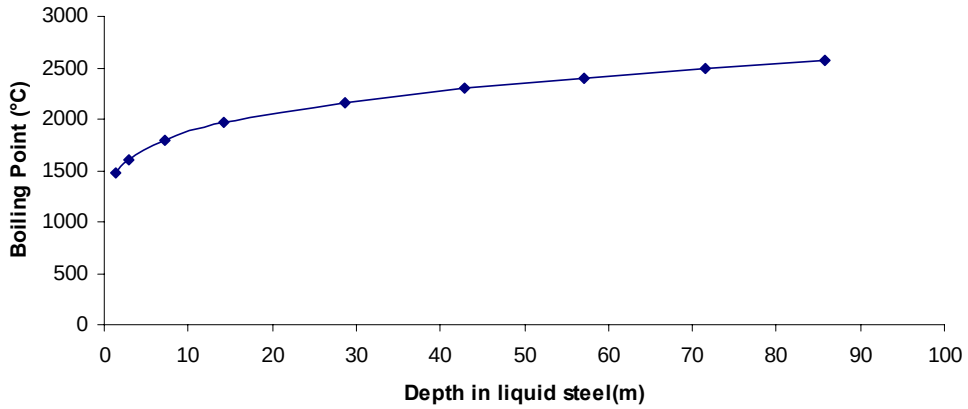

Figure 1.10. The variation of the boiling point of calcium with the depth of the wire in liquid steel

Also, Ca-wire injection provides for a better Ca-reaction with the liquid metal because of the formation of a steel shell around the wire allowing it to be injected deep into the bath before the Ca begins to vaporize. In addition, due to the fast rate of injection, the wire is deep in the molten steel before vaporization occurs [19]. Figure 1.11 shows a schematic diagram of Ca wire injection into a ladle.

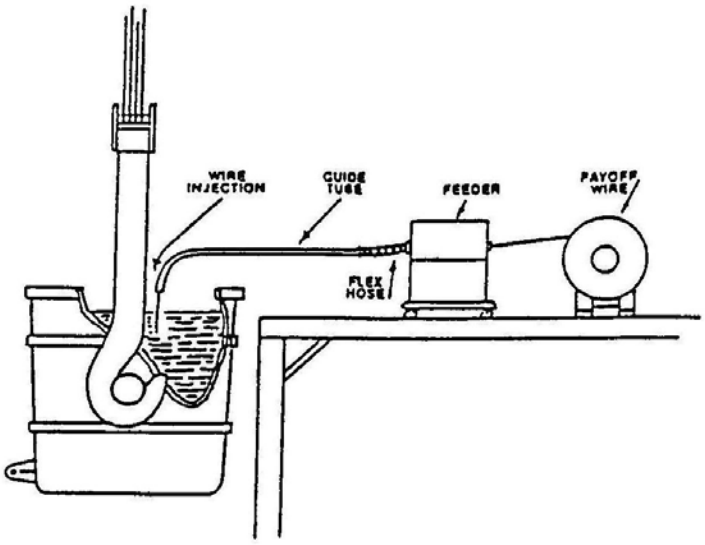

Figure 1.11. Schematic diagram of Ca wire injection into a ladle [19]

1.4. OUTLINE OF THE PROJECT

The literature review indicates that the presence of inclusions in steel castings is harmful for the mechanical properties of steel. These inclusions can be reduced or modified to produce “clean” steel by using optimal deoxidation and pouring practices. There has not been sufficient research in this area, with respect to small steel foundries, of capacity 1 to 20 tons.

The amount, size, distribution, shape, and composition of inclusions are important to evaluate steel cleanliness. In the past, several researchers have been measuring inclusions in microscopic steel specimens with the help of scanning electron microscopy (SEM) analysis combined with energy dispersive spectroscopy (EDS). However, manual

SEM approaches are limited by the labor intensive nature of the analysis because the SEM operator must analyze by manually imaging the individual inclusions.

In order to increase the speed and efficiency of inclusion evaluation, this research uses an automated inclusion analyzer, ASPEX PICA-1020. This equipment provides a rapid and accurate method for determining the composition, size, number, spacing and distribution of inclusions present in the steel samples. It is an integrated SEM and EDS system and allows for automated characterization of all the inclusions (1 μm to 5 mm) in a microscopic specimen; including the volume fraction, size and shape, inclusion spacing and complete inclusion identification.

The main objective of this research is to suggest the optimum deoxidation and ladle-practices in steel foundries which minimizes harmful inclusions in the steel casting. This is done by evaluating the various steel foundry practices in terms of inclusions, oxygen content and toughness of the cast product.

2. BENCHMARKING CASTING PRACTICES

2.1. BACKGROUND OF ASPEX ANALYSIS

In the Aspex system, a focused electron beam searches for features in a user specified region. The region can be defined by a circle, a polygon or a list of stage points. The selected region is then subdivided into smaller fields. For example, a 4x4 mm square sample field can be broken down into 16 fields of 1x1mm square that are defined electronically as illustrated in Figure 2.1. This figure shows the difference between the search grid and the measurement grid. The red regions represent features, the larger black dots represent search points and the small dots represent measurement points. The larger spacing between search grid steps misses the upper-left feature but finds both the central and lower-right feature. Once a feature has been found, the steps size is reduced to more precisely measure the feature dimensions. The large search steps lead to fast searches while the small measurement steps lead to precise measurements. This is a fast process because the instrument only spends time collecting detailed sizing data where inclusions are known to be present, rather than spending time capturing and analyzing vast numbers of essentially empty pixels.

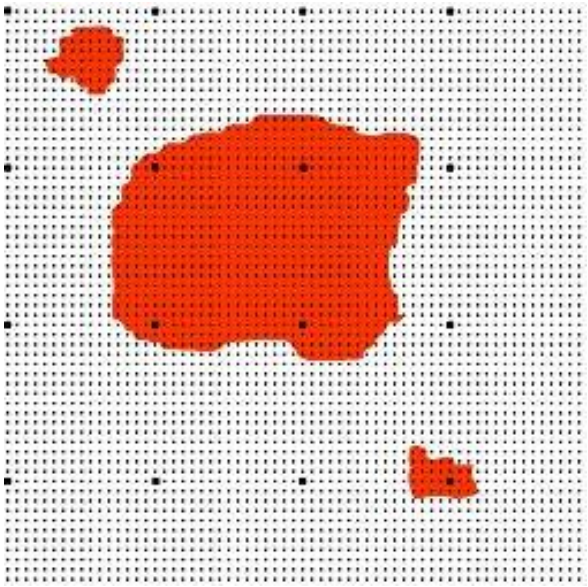

Figure 2.1. The measurement grid of the Aspex beam with both the big dots showing the coarse step size and the small dots showing the fine step size [24]

As the electron beam moves across each field, the brightness or intensity of the back scattered electron detector (BSED) signal is recorded and transferred to the computer memory as representing the brightness of a single pixel. If the signal is bright enough to indicate that an inclusion is present at the position, the software initiates a particle-sizing sequence using a rotating chord algorithm. Figure 2.2 shows an example of the rotating chord algorithm. The rotating chord algorithm finds the center of the feature and draws 16 chords through the center at approximately 11-degree intervals. A number of metric parameters are computed from the lengths of the chords including average, maximum and minimum diameters, orientation and centroid.

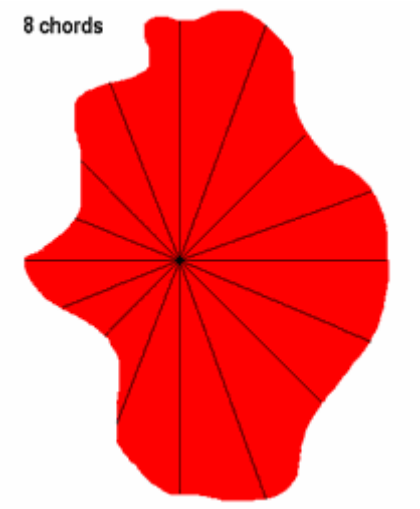

Figure 2.2. This figure shows a representative image of a feature with 8 chords drawn through the centroid to the edges of the feature [24]

After inclusions have been fully characterized for size and shape, an EDS spectrum is acquired to determine the elemental composition of each inclusion. After the sample had been completely analyzed and the data stored, the data was evaluated offline by the Automated Feature Analysis software.

In order to extract meaningful interpretations from the numerous compositional and morphological parameters, the data obtained is sorted into classes. The inclusions are classified into various classes based on their composition as determined by user-defined

rules. Rules provide a mechanism to define membership classes based on chemical or morphological properties. For example, an inclusion lying in the range of 1µm - 50µm with Mn >= 30% and S >=20% is classified as a MnS inclusion. The standard rules defined and used for this study are given in Appendix A.

In addition to the other types of analysis, binary and ternary mappings of the oxide and sulfide inclusions are available for pointing out their dominant composition, as shown in Figure 2.3. These illustrations are often very helpful to get an overview of the inclusion composition in the sample. They can also help in determining the morphological and chemical changes associated with melting and ladle practices.

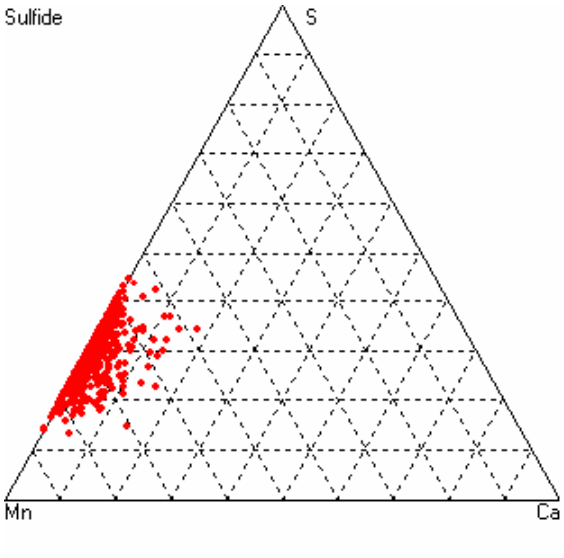

Figure 2.3. Ternary mapping of Mn-Ca-S in sulfide inclusions

In order to measure the spacing between the inclusions through Aspex, all the coordinates of the inclusions were transported to a Microsoft Excel file and a code was written in Visual Basic software. This code first calculates the distance of an inclusion from each of the other inclusions and determines the distance to the closest neighbor. These distances are averaged over all inclusions to determine the average spacing between the inclusions in the specimen. The Visual Basic code is given in Appendix B.

2.2. EXPERIMENTAL PROCEDURE

Plant trials were conducted at four foundries with different deoxidation practices in the furnace and ladle as summarized in Table 2.1. Three foundries were induction furnace based (IF) and one foundry had acid and basic electric arc furnaces (EAF). Table 2.2 gives the chemistry of all the heats tested for the different plants, as provided by the plants.

Table 2.1. Melting and deoxidation practices at the four foundries

	Charge Weight (lbs.)	Furnace additions (in wt. %)	Ladle additions (in wt. %)
Plant A (IF)	1000	-	Added at tap: Al (0.1%) FeTi (0.035% Ti) FeSiZr (0.04% Si, 0.03% Zr)
Plant B (IF)	1400	Al (0.08%)	Added at tap: CaSi(0.08% Ca, 0.3% Si)
Plant C (Acid EAF)	40,000	FeMn+FeSi Block additions	Added at tap: Al (0.07%) Wire fed in ladle CaSi (0.06% Ca, 0.10% Si)
Plant C (Basic EAF)	40,000	FeMn+FeSi Block additions	Added at tap: Al (0.068%) Wire fed in ladle CaSi (0.04% Ca, 0.08% Si)
MS&T Foundry (IF)	100	Al (0.10%)	Added at tap: CaSi(0.09% Ca, 0.17% Si)

During the plant trials, the dissolved oxygen content was measured directly in the liquid steel, using Celox oxygen probes and the Celox Lab Datacast-2000. Steel samples

were collected from the furnace and the ladle using vacuum chemistry samplers, before and after the addition of deoxidants. In addition, samples were cut from cast keel blocks produced from the same heat. Microscopic specimens were prepared from these samples and a 10 mm^2 area was analyzed in each specimen for inclusions using the Aspex PICA-1020 for automated inclusion analysis. Each sample was analysed on the Aspex five times, in order to check the accuracy of the inclusion measurements within a single sample. The total oxygen content was measured from each sample using Leco TC-500.

Table 2.2. Chemistry of all the heats tested as provided by the plants

	C	Mn	P	S	Si	Cu	Ni	Cr	Mo	V	Al
Plant A (IF)	0.30	0.71	0.01	0.037	0.45	0.06	0.05	0.175	0.04	0.007	0.07
Plant B (IF)	0.28	0.80	0.03	0.04	0.50	0.05	0.04	0.15	0.03	0.01	-
Plant C (Acid EAF)	0.30	0.98	0.01	0.015	0.56	0.15	0.16	0.28	0.03	0.015	0.02
Plant C (Basic EAF)	0.30	1.10	0.01	0.009	0.45	0.15	0.21	0.20	0.05	0.015	0.01
MS&T Foundry (IF)	0.41	0.70	0.01	0.037	0.48	0.15	1.6	0.82	0.23	-	-

2.3. RESULTS AND DISCUSSION

2.3.1. Plant A. In the trial at Plant A, a heat of medium-carbon steel (WBC) was produced in an induction furnace (IF) and tapped into a 1000 lb capacity ladle. The practice included deoxidation in the IF with 1 lb Al, followed by a complex treatment of

1 lb of Al, 0.66 lbs of Fe70Ti alloy and 0.88 lbs of Fe51Si35Zr alloy in the ladle during tap. Ti and Zr are both stable nitride-formers and added to minimize AlN embrittlement [25]. Figure 2.4 (a and b) compare the area fraction covered by inclusions and the total and dissolved oxygen, at the various stages of liquid processing. The average size and aspect ratio of the inclusions at all the stages, as measured by Aspex, are given in Figure 2.4 (c and d).

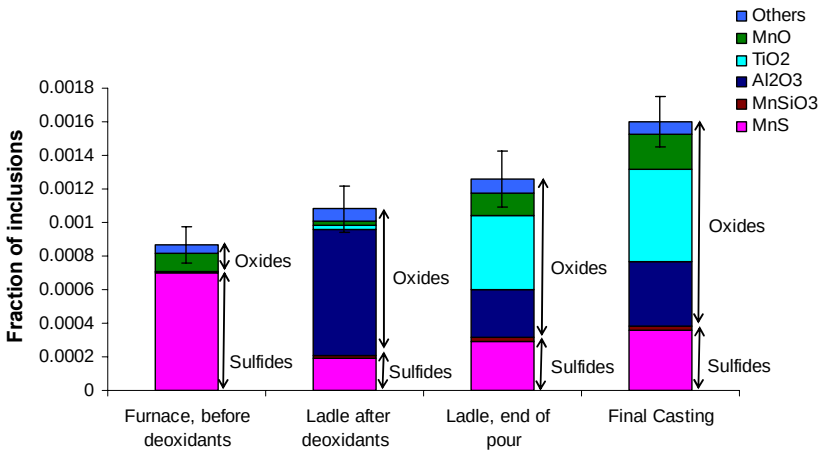

a)

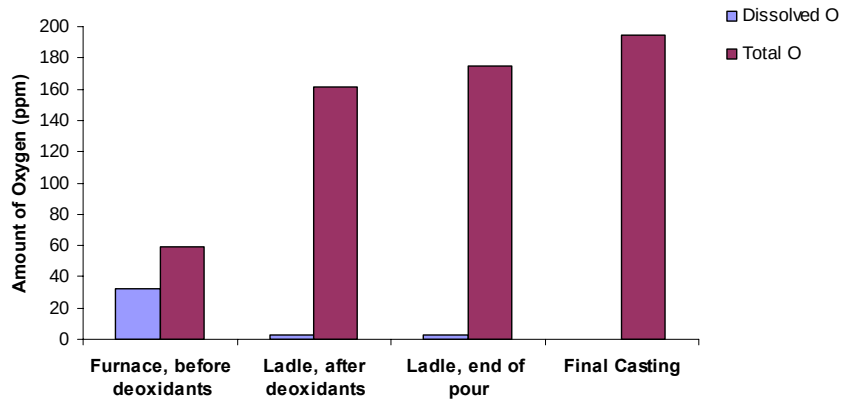

b)

Figure 2.4. Comparison of a) inclusion volume, b) dissolved and total oxygen, c) average inclusion size, and d) average inclusion aspect ratio measured in samples collected at various stages of the casting process (Plant A)

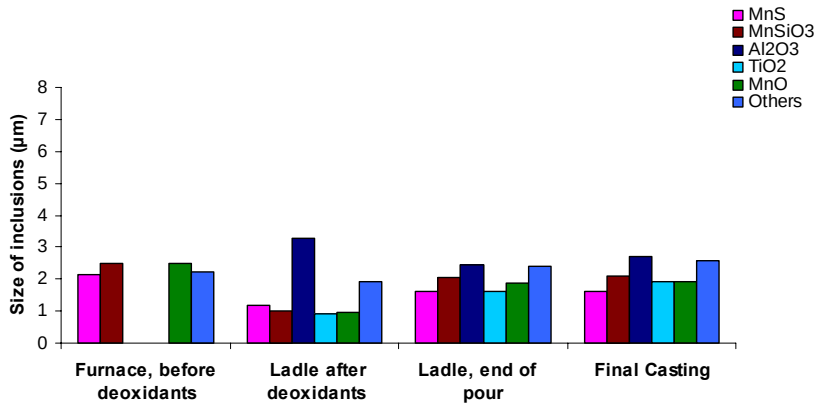

c)

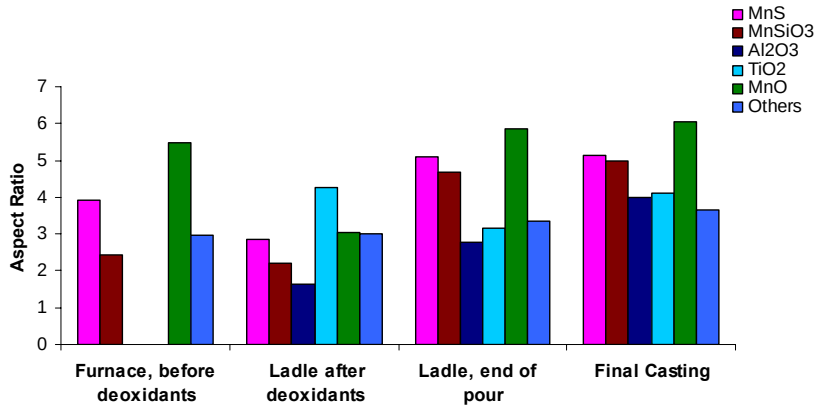

d)

Figure 2.4. Comparison of a) inclusion volume, b) dissolved and total oxygen, c) average inclusion size, and d) average inclusion aspect ratio measured in samples collected at various stages of the casting process (Plant A) (cont.)

The area fraction represents the fraction of the area covered by inclusions in a 10 mm^2 microscopic specimen. The area fraction of oxide inclusions increased during the pour and resulted in the highest area fraction of inclusions in the final casting (Figure 2.4 a). This indicates that there is significant reoxidation during pouring and in liquid metal transport through the gating system. Also, there is insufficient time to float out inclusions in the ladle. The dissolved oxygen dropped after deoxidation, resulting in the formation of a large number of oxide inclusions and an increase in the total oxygen. The total oxygen continued increasing towards the end of the pour indicating reoxidation and a lack of inclusion flotation (Figure 2.4 b).

The area of alumina and TiO_2 inclusions increased after the Al and FeTi additions in the ladle. There was some reduction in the alumina inclusions towards the end of the pour, but TiO_2 inclusions continued to increase through casting. TiO_2 inclusions are difficult to float out due to their small size and irregular shape as compared to the agglomerate of alumina inclusions. In the sample collected from the ladle after deoxidation, the average diameter of the TiO_2 inclusions was 1.5 μm with a 4.5 aspect ratio, significantly smaller and less round than the alumina inclusions which had an average size of 3 μm with an aspect ratio of 1.5 (Figure 2.4 c and d). Smaller inclusions are difficult to float out, as shown with FLUENT modeling (Figure 3.5 in Section 3.3).

2.3.2. Plant B. In this plant trial, one induction furnace heat was followed from melting through deoxidation and pouring of a medium-carbon steel (8625 alloy) in a 1400 lb ladle. For deoxidation, Al was added in the furnace just before tap followed by bulk CaSi addition in the tap stream.

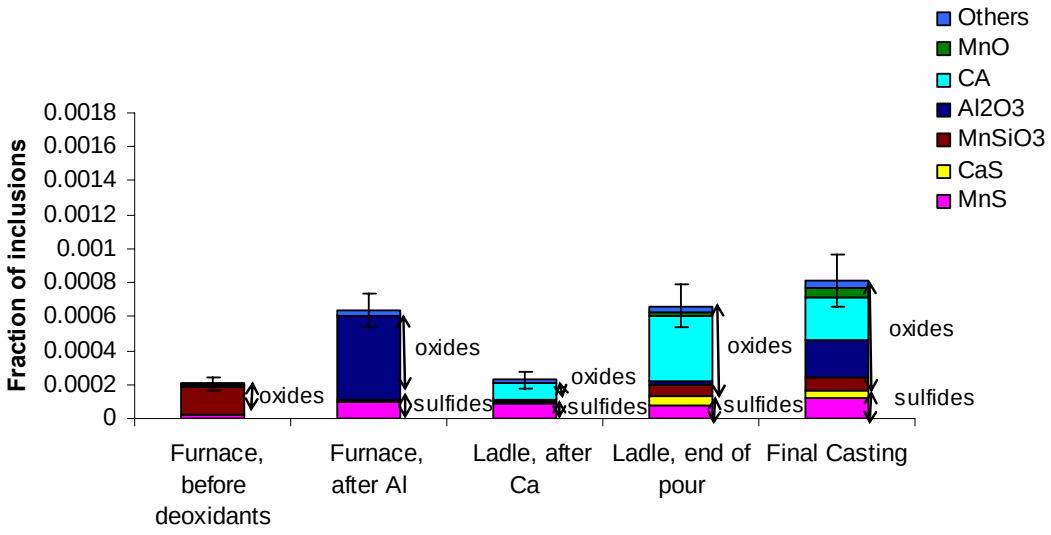

a)

Figure 2.5. Comparison of a) inclusion volume, b) dissolved and total oxygen, c) average inclusion size, and d) average inclusion aspect ratio measured in samples collected at various stages of the casting process (Plant B)

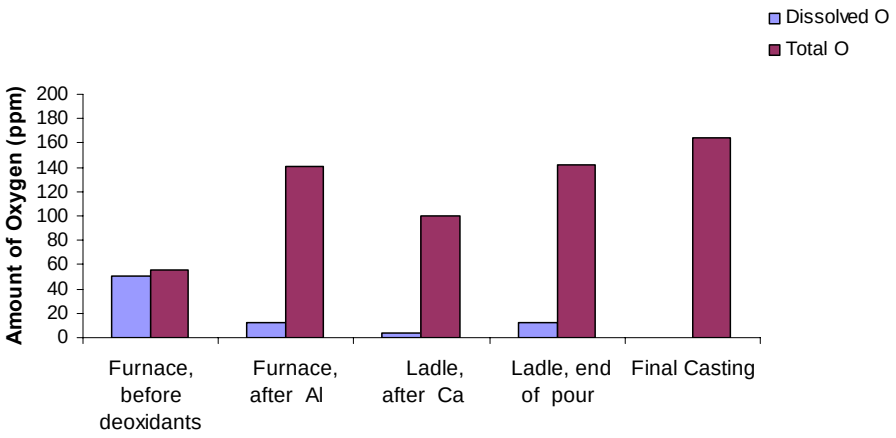

b)

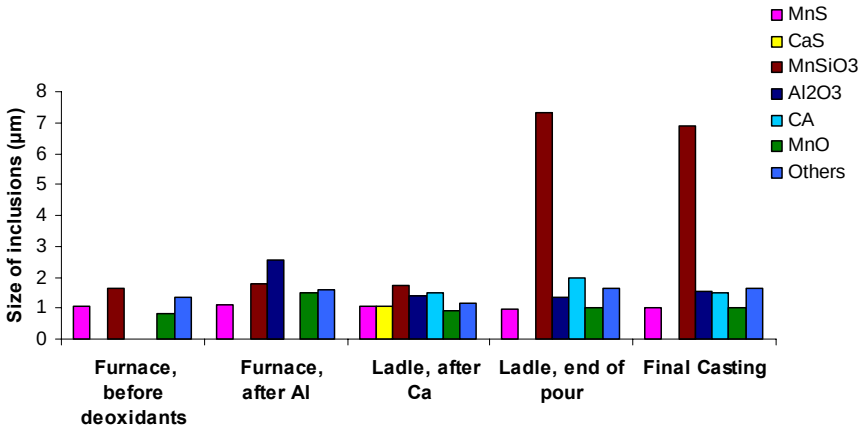

c)

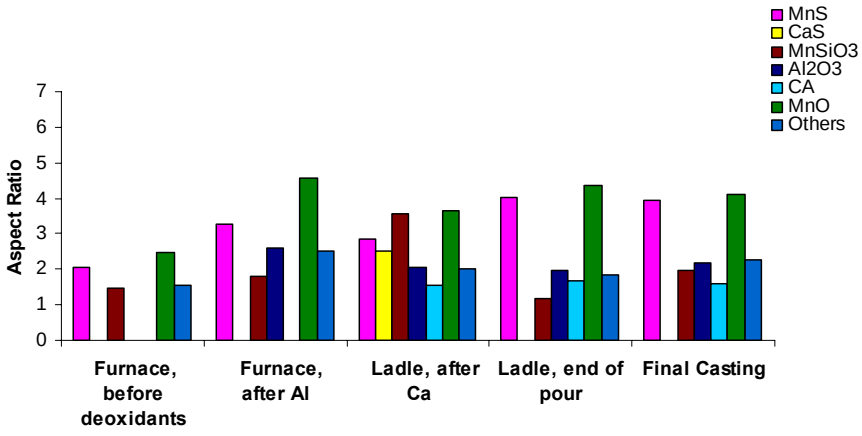

d)

Figure 2.5. Comparison of a) inclusion volume, b) dissolved and total oxygen, c) average inclusion size, and d) average inclusion aspect ratio measured in samples collected at various stages of the casting process (Plant B) (cont.)

After Al treatment in the furnace, there was an increase in the alumina inclusions and the total oxygen (Figure 2.5 a and b). The composition and number of inclusions changed after the Ca treatment in the ladle with most of the alumina inclusions forming calcium aluminates (CA). This modification is good because calcium aluminate inclusions have lower aspect ratio than alumina inclusions and, hence, are less harmful to mechanical properties of steel (Figure 2.5 d). MnS inclusions were first observed in the furnace and remained fairly constant, in terms of number, shape and size, through the ladle and casting. This shows that the Ca-treatment was not able to modify the MnS inclusions. Significant reoxidation was observed with all the oxide inclusions increasing from the ladle through casting, specially $MnSiO_3$ inclusions show a huge increase in size at the end of the pour and in the final casting (Figure 2.5 c).

Figure 2.6 shows the ternary chemical mapping for a) sulfides and b) oxides before and after Ca additions in the ladle, as obtained through Aspex. The region of calcium aluminates (CA) is marked on the ternary oxides diagram.

In the ternary oxide mapping Ca modification of the alumina inclusions was observed, but there was limited Ca modification of the MnS inclusions, as seen in the ternary sulfide mapping. Adding Ca in the form of a CaSi ferroalloy during tap is inconsistent in its metallurgical effectiveness. The CaSi ferroalloy was observed to float on the liquid metal surface often flashing indicating vaporization of Ca followed by rapid combustion in air. Ca is highly volatile with a boiling point of $1491^{o}C$ making it difficult to add to the steel without losing it to vaporization. Injection of calcium below the surface of the steel through wire or powder injection would be more effective as it suppresses Ca boiling because of the higher ferrostatic pressure [19]**.**

2.3.3. Plant C. In this study, two electric arc furnace heats of medium-carbon steel were followed, with ladle of capacity 20 tons. The first one utilized an acid refractory and slag practice and the second one used a basic refractory and slag practice. Ladle treatment included preliminary deoxidation during tap followed by treatment with Ca wire in the ladle. During the heat, chemistry samples and dissolved oxygen readings were collected at the following locations: 1) furnace after block, 2) ladle before calcium wire treatment, 3) ladle after calcium wire treatment, 4) ladle at mid-ladle pouring, and 5) cast product.

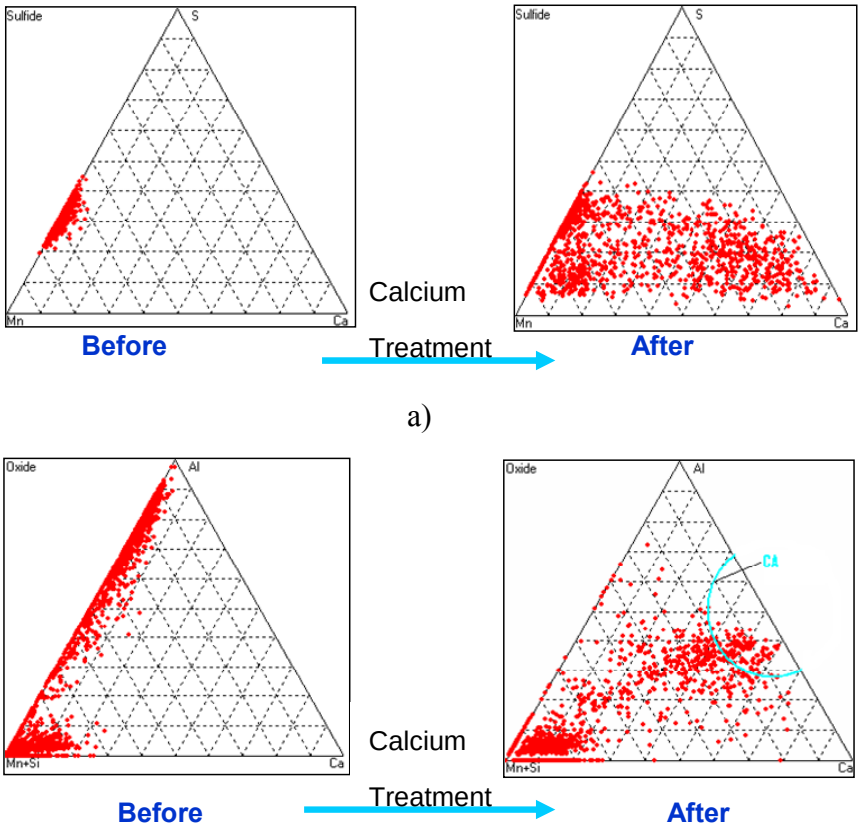

Figure 2.6. a) Sulfides Mn-Ca-S and b) oxides (Mn+Si)-Ca-Al mapping for the casting process, before and after addition of Ca in the ladle (Plant B)

In the acid process, the area of inclusions decreased after addition of the Ca due to the formation of calcium aluminates (CA) and MnS inclusions were modified to CaS inclusions (Figure 2.7a). Ca-treatment helped in decreasing the oxygen content too, even though the oxide inclusions continued increasing towards the end of the casting process (Figure 2.7b). Figure 2.7 d) shows the effect of Ca-treatment on the aspect ratio of the inclusions. It is interesting to see that the Ca-modified inclusions, calcium aluminate and CaS, have a lower aspect ratio than the alumina and MnS inclusions, showing that Ca-treatment is beneficial in not only decreasing the inclusions but also in giving the inclusions a globular shape. Figure 2.7 c) shows that there are some huge Al_2O_3, MnO, and $MnSiO_3$ inclusions in the earlier stages of the casting process, but these inclusions are easily floated out towards the end of the casting due to their large size.

In the basic process, many of the alumina and MnS inclusions were not successfully modified by calcium (Figure 2.8 a). This can be explained as more CaSi wire was added to the ladle in the acid process (0.06 wt. % Ca) as compared to the basic process (0.04 wt. % Ca). The amount of Ca in the basic process was not sufficient to cause the modification of MnS and alumina to CaS and calcium aluminate inclusions, respectively. As a result, there is no significant reduction in total oxygen too, as seen in Figure 2.8 b). The average size of the inclusions (Figure 2.8 c) is less here as compared to the acid process and overall, the acid process had more inclusions than the basic process, which is supported by the higher levels of total oxygen. Also, the small amount of modified calcium inclusions show a low aspect ratio (Figure 2.8 d), suggesting that an adequate amount of Ca-addition would have helped in floatation and modification of inclusions in the basic process too.

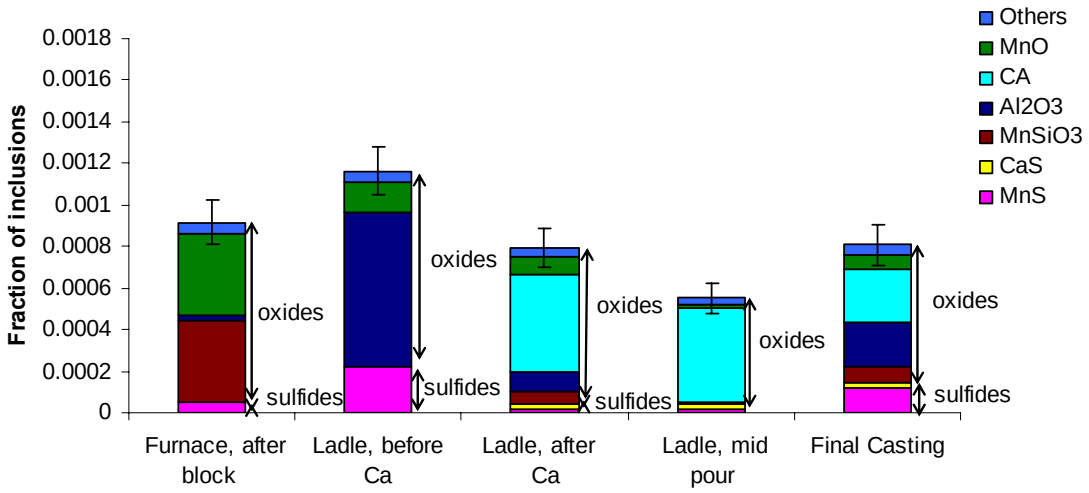

a)

Figure 2.7. Comparison of a) inclusion volume, b) dissolved and total oxygen, c) average inclusion size, and d) average inclusion aspect ratio measured in samples collected at various stages of the casting process (Plant C-acid)

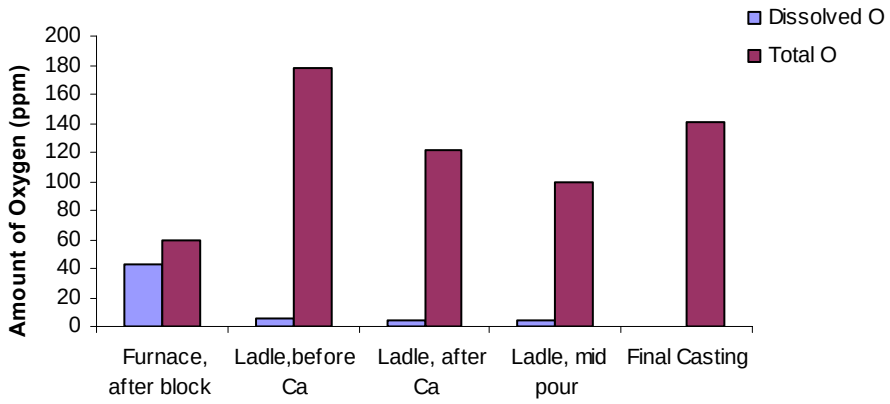

b)

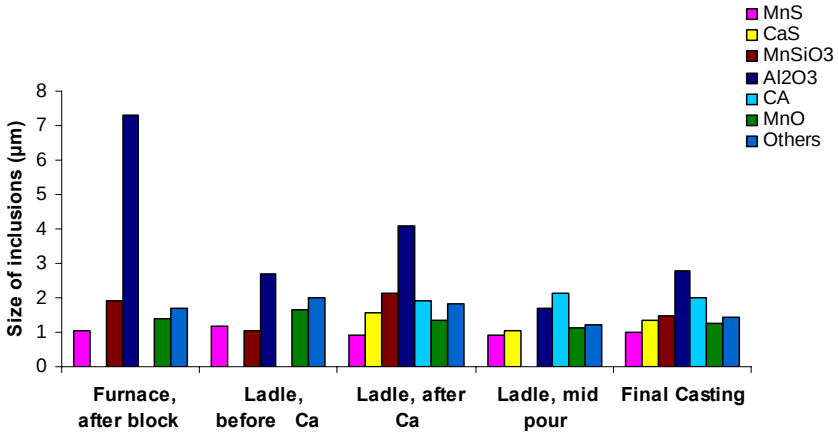

c)

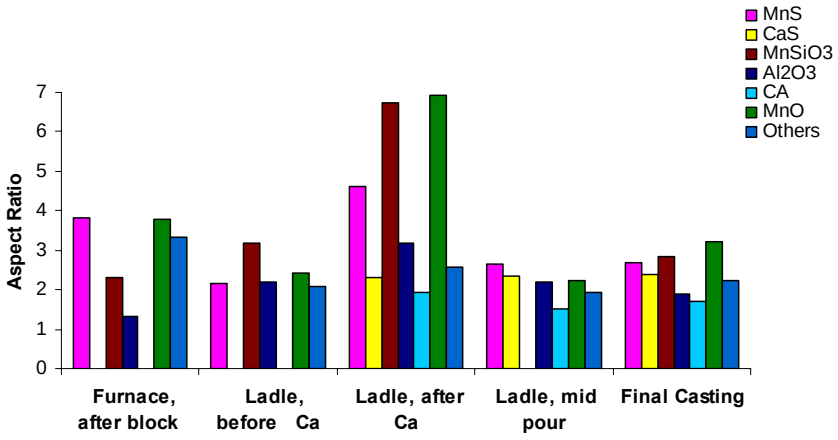

d)

Figure 2.7. Comparison of a) inclusion volume, b) dissolved and total oxygen, c) average inclusion size, and d) average inclusion aspect ratio measured in samples collected at various stages of the casting process (Plant C-acid) (cont.)

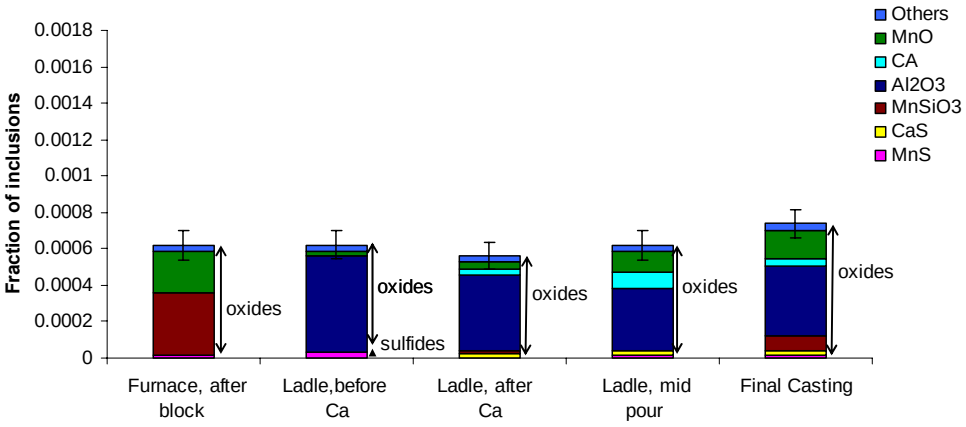

a)

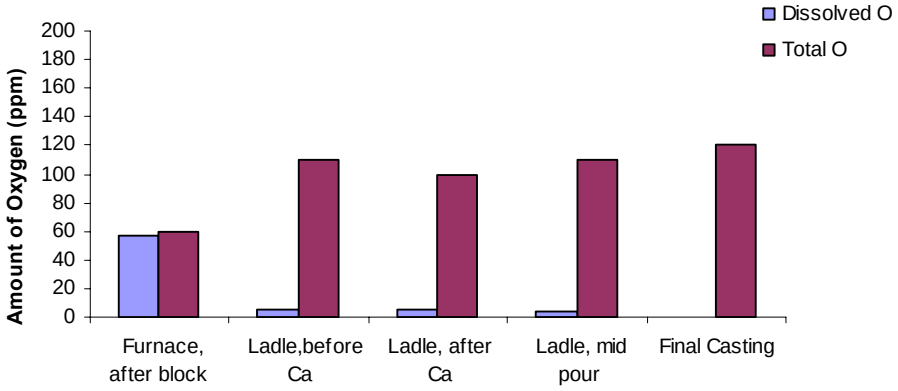

b)

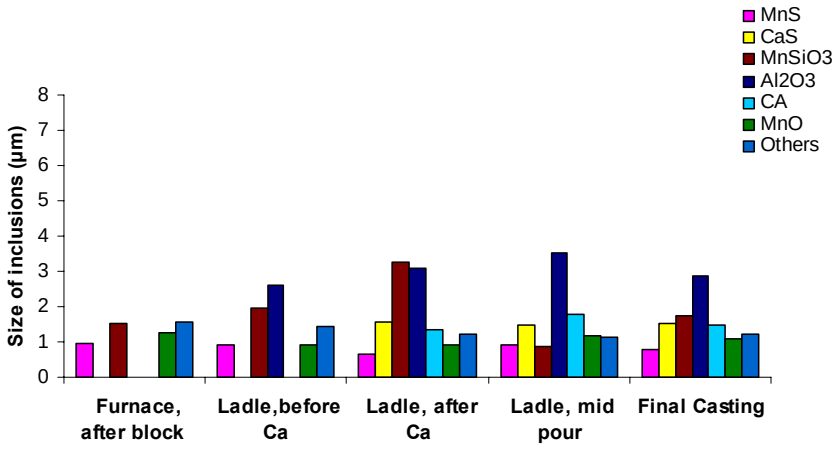

c)

Figure 2.8. Comparison of a) inclusion volume, b) dissolved and total oxygen, c) average inclusion size, and d) average inclusion aspect ratio measured in samples collected at various stages of the casting process (Plant C-basic)

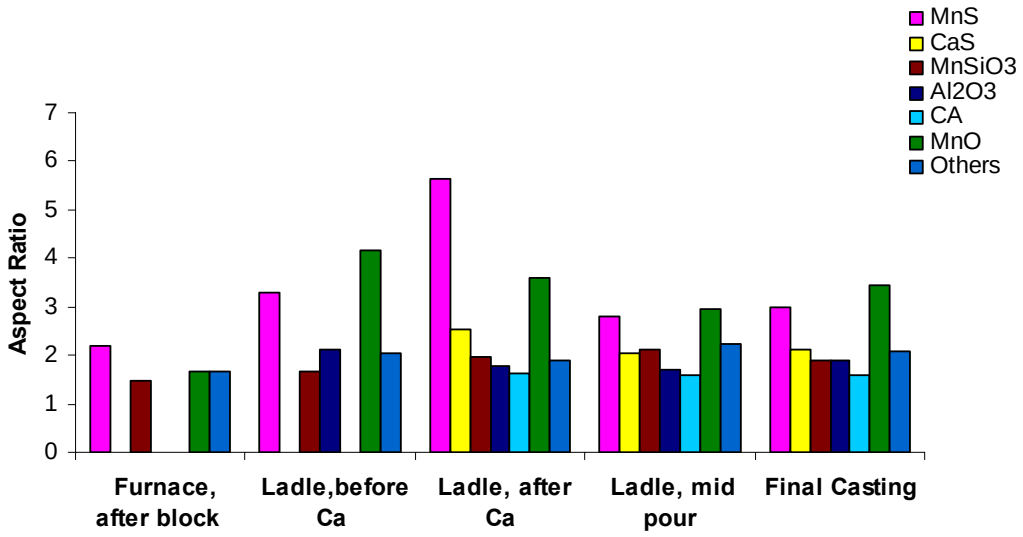

d)

Figure 2.8. Comparison of a) inclusion volume, b) dissolved and total oxygen, c) average inclusion size, and d) average inclusion aspect ratio measured in samples collected at various stages of the casting process (Plant C-basic) (cont.)

Figure 2.9 summarizes the inclusion composition for the acid process using a ternary mapping system for sulfides and oxides. After the Ca addition, the fraction of MnS inclusions decreased and was replaced by CaS inclusions. This is a desired transformation due to the globular morphology of CaS, which can be observed in Figure 2.7 d). Also, a significant amount of CA formation was observed with a decrease in both MnO and Al_2O_3 inclusions. Figure 2.10 presents a binary phase MnS-CaS diagram, which shows that MnS and CaS could form a solid solution above 1150^{o}C. Figure 2.11 verifies the presence of a MnS-CaS inclusion, which was obtained through Aspex, from the final casting sample collected from the acid practice of this plant. This transformation of MnS to MnS-CaS solutions and relatively pure CaS was also observed in the Mn-Ca-S inclusion mapping (Figure 2.9 a).

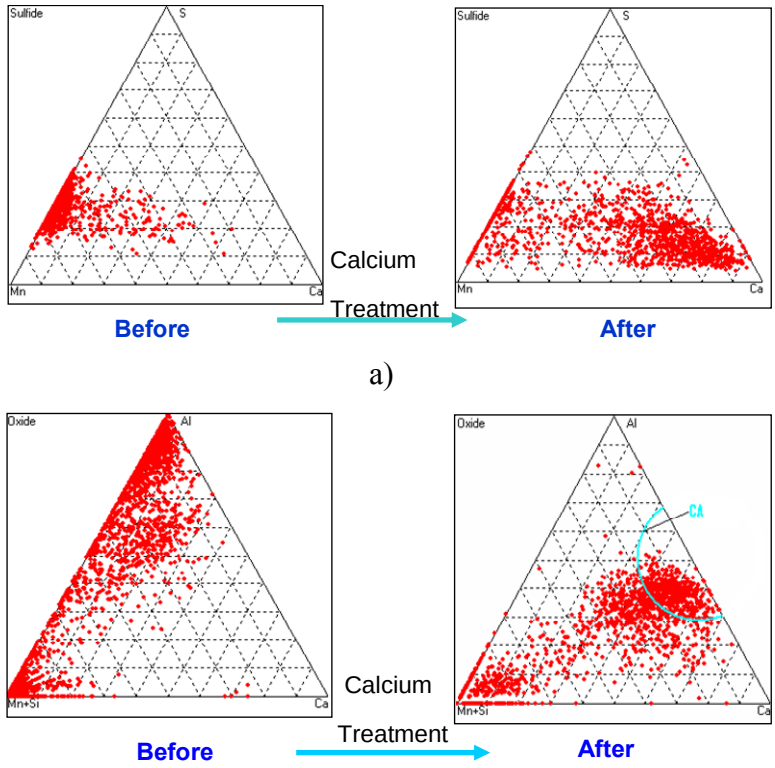

Figure 2.9. a) Sulfides *Mn-Ca-S* and b) oxides *(Mn+Si)-Ca-Al* mapping for casting process, before and after addition of *Ca* in the ladle (Plant C, Acid process)

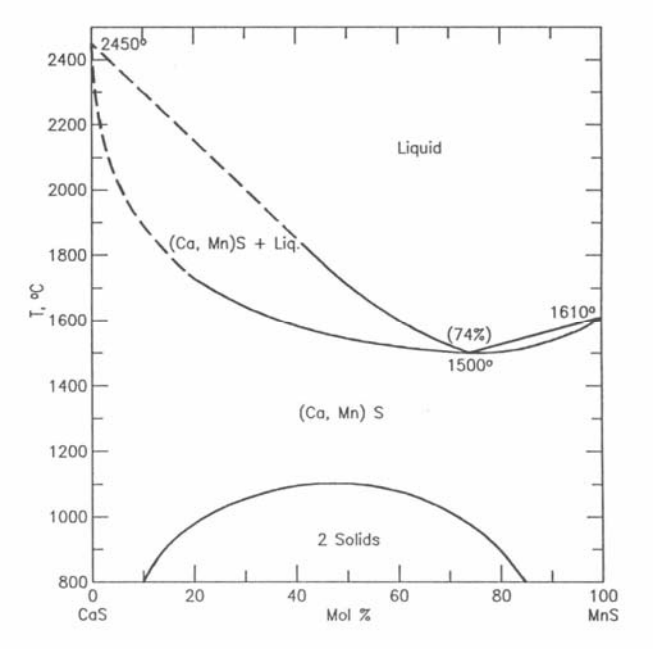

Figure 2.10. Binary MnS-CaS phase diagram [26]

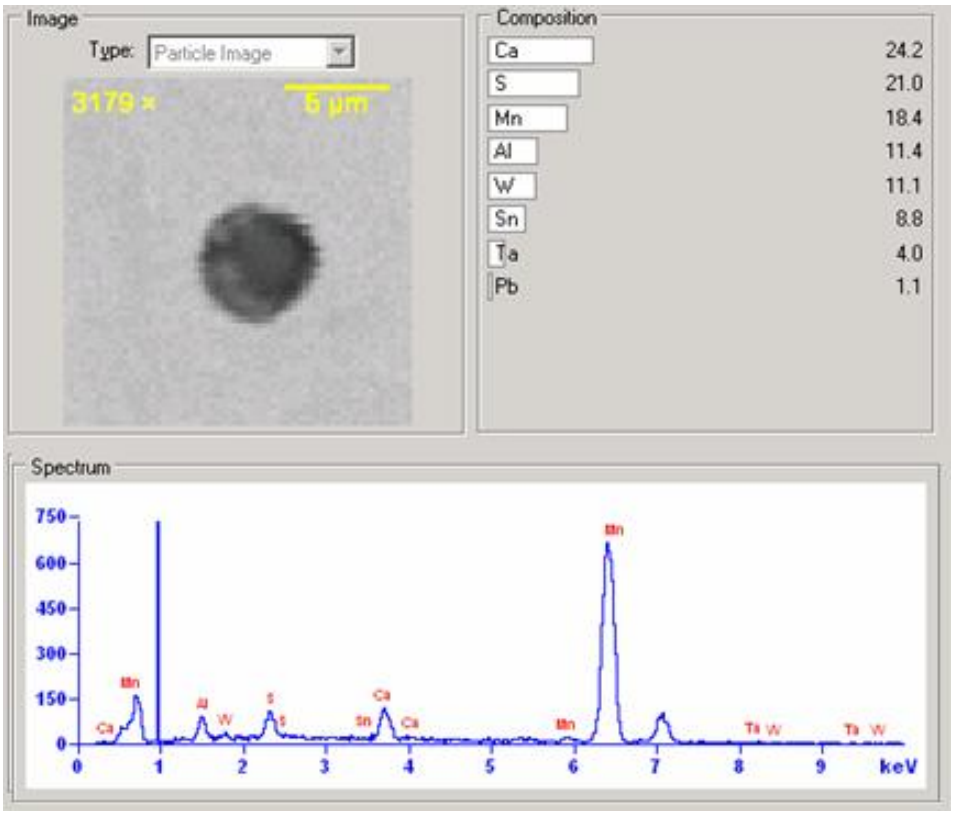

Figure 2.11. SEM and EDS image of a MnS-CaS inclusion, from the final casting sample collected from the acid process of plant C, obtained through Aspex PICA-1020

Figure 2.12 shows the ternary chemical mapping of the sulfide and oxide inclusions for the basic process. Contrary to the acid practice, there was not much of a decrease in MnS and Al_2O_3 inclusions in the basic practice. Also, any significant formation of the desired CaS or CA inclusions was not observed in the basic process.

Figure 2.13 a) and b) show the non-spherical shapes of MnS and Al_2O_3 inclusions obtained from the sample collected before Ca-treatment in the ladle in the acid practice. For the same heat, the sample collected from the ladle after the Ca-treatment showed the presence of spherical CaS and CA inclusions, as seen in Figure 2.14 a) and b). The reduction in the shape factor of the inclusions with Ca-treatment in the acid practice is observed in Figure 2.7 d).

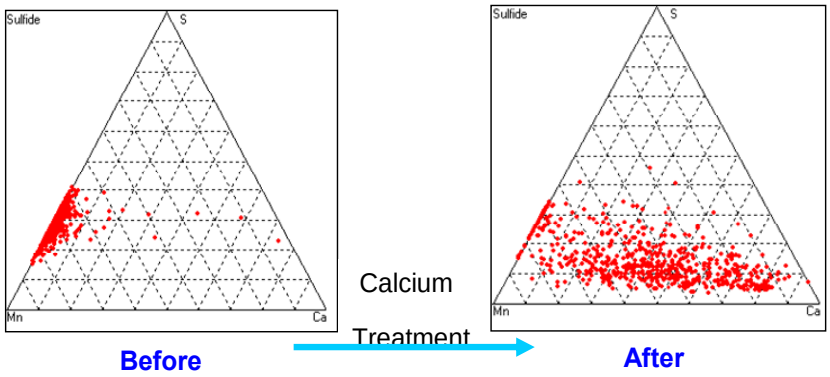

a)

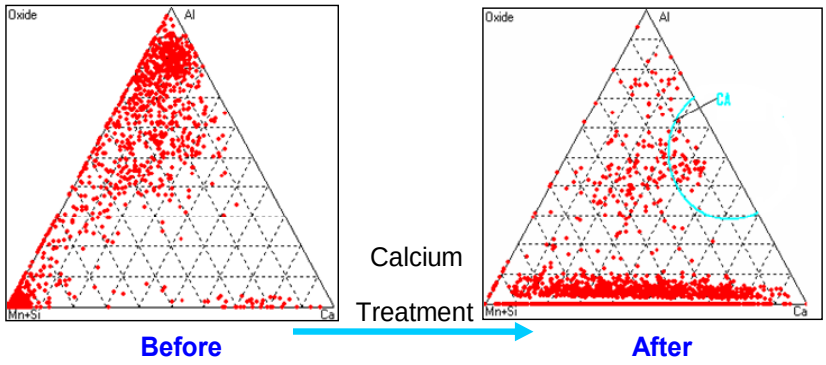

b)

Figure 2.12. a) Sulfides *Mn-Ca-S* and b) oxides *(Mn+Si)-Ca-Al* mapping for casting process, before and after addition of *Ca* in ladle (Plant C, basic)

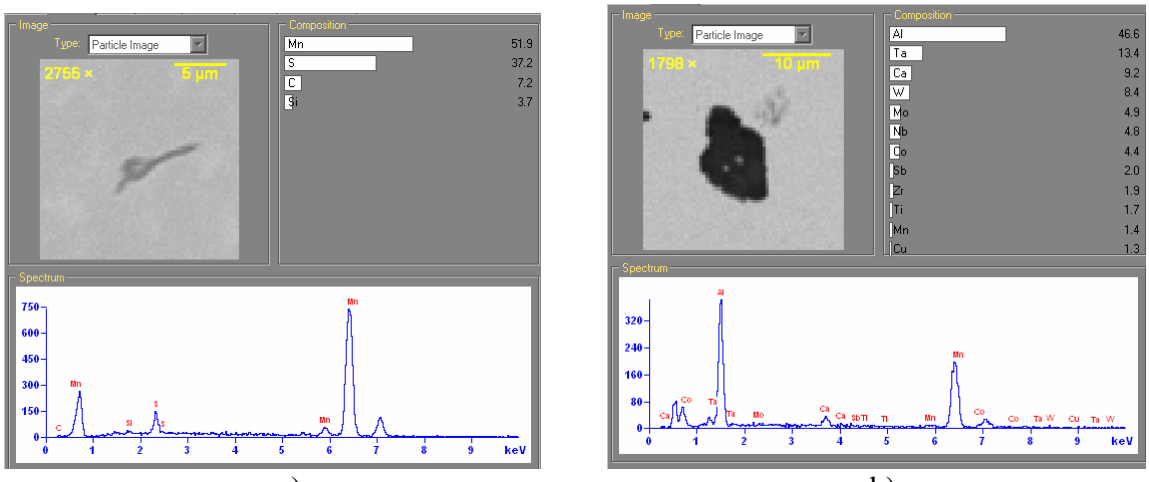

a) b)

Figure 2.13. SEM and EDS images of non-spherical a) MnS and b) alumina inclusions from the sample collected before Ca-treatment in the ladle in the acid practice, obtained through Aspex PICA-1020

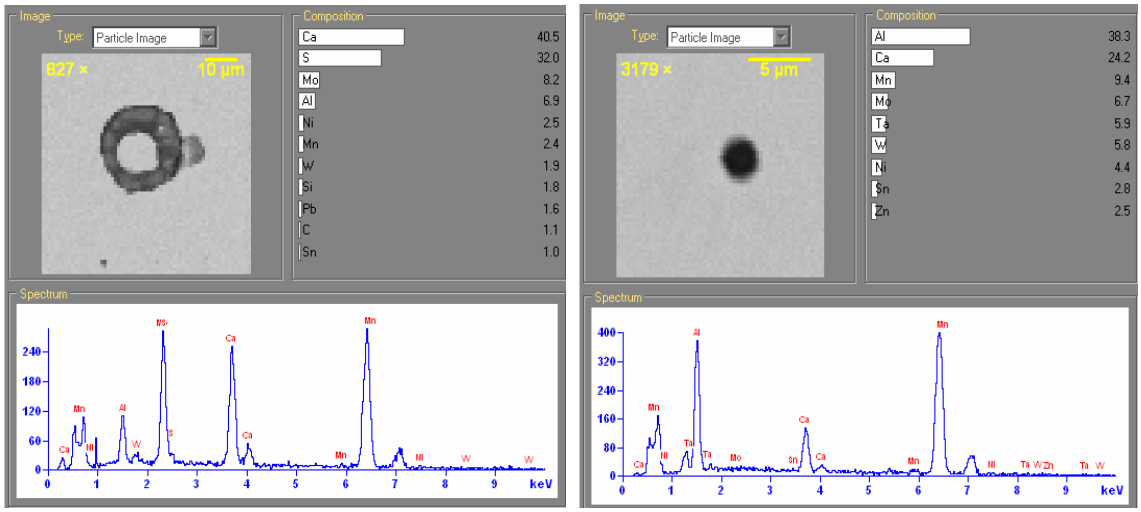

a) b)

Figure 2.14. SEM and EDS images of spherical a) CaS and b) calcium aluminate inclusions from the sample collected after Ca-treatment in the ladle in the acid practice, obtained through Aspex PICA-1020

2.3.4. Missouri S&T Foundry. A heat of medium-carbon (4340) steel was melted in the Missouri S&T 100 lb induction furnace. Aluminum was added in the furnace just before tap followed by a calcium silicon addition in the tap stream for deoxidation.

Alumina inclusions increased after the addition of Al in the furnace, with a significant increase in the total oxygen also (Figure 2.15a and b). With Ca-treatment in the ladle, most of the alumina inclusions form calcium aluminates (CA), but the MnS inclusions remain almost constant and are not completely modified to CaS inclusions. This is due to the ineffective addition of CaSi during tap in small ladle, which does not allow the Ca to interact with the liquid steel before vaporizing. The oxide inclusions, and the total oxygen, increased from the ladle to the casting, indicating that there was reoxidation during the pouring. There was significant increase in the size of the $MnSiO_3$ inclusions in the casting sample (Figure 2.15 c). The modified inclusions after Ca-treatment, that is, the CA and CaS inclusion had aspect ratios close to 1, showing that Ca-treatment helps in giving inclusions a spherical morphology (Figure 2.15 d).

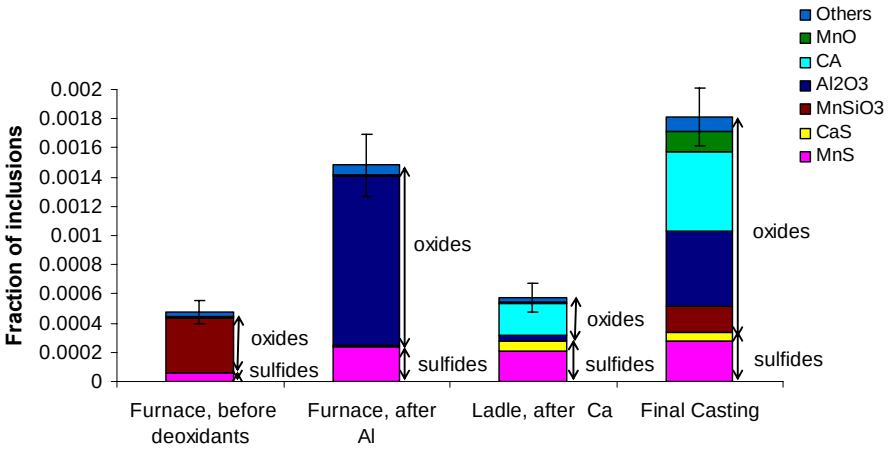

a)

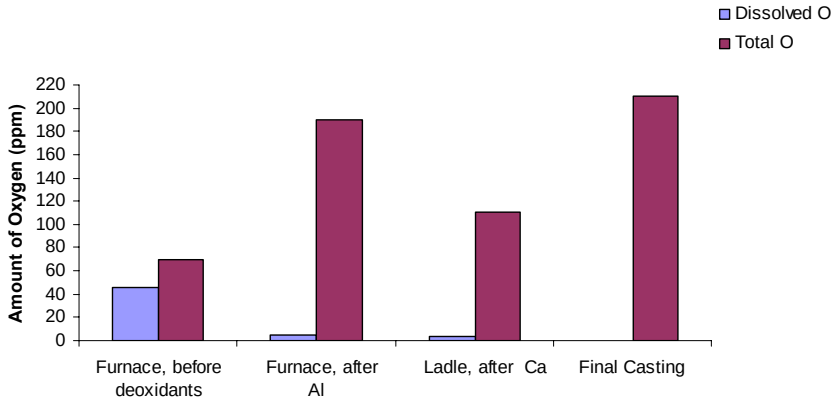

b)

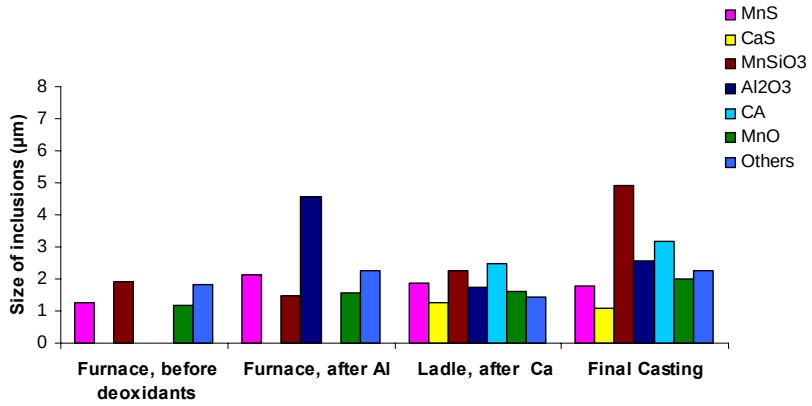

c)

Figure 2.15. Comparison of a) inclusion volume, b) dissolved and total oxygen, c) average inclusion size, and d) average inclusion aspect ratio measured in samples collected at various stages of the casting process (MS&T foundry)

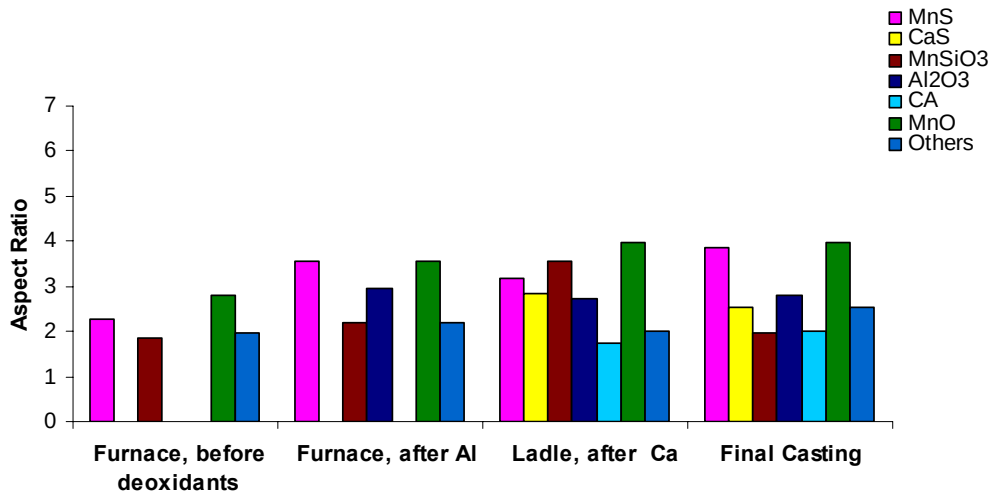

d)

Figure 2.15. Comparison of a) inclusion volume, b) dissolved and total oxygen, c) average inclusion size, and d) average inclusion aspect ratio measured in samples collected at various stages of the casting process (MS&T foundry) (cont.)

2.3.5. Effect of Different Practices on Inclusions. This section summarizes the results obtained from the plant trials conducted at the different foundries. The effects of the different melting and ladle practices is compared with respect to the inclusion volume, shape, size and spacing

2.3.5.1. Effect of Ca-addition. Figure 2.16 compares the no calcium-treatment process in Plant A with the bulk CaSi-addition in Plant B. Both had ladles of comparable size, but Ca-treatment helped modify MnS to CaS and transformed alumina to calcium aluminates (CA). CaSi addition helped in decreasing the inclusion content in the cast sample (Figure 2.16 a). The size and aspect ratio was found to be lesser for the Ca-treated plant B samples, suggesting that calcium helps in controlling the shape and the size of the inclusions (Figure 2.16 b and c). The difference between their shape and size decreased towards the later stages of the casting, because reoxidation affected the aspect ratio and the size of the inclusions significantly, hence diminishing the effect of the Ca-treatment.

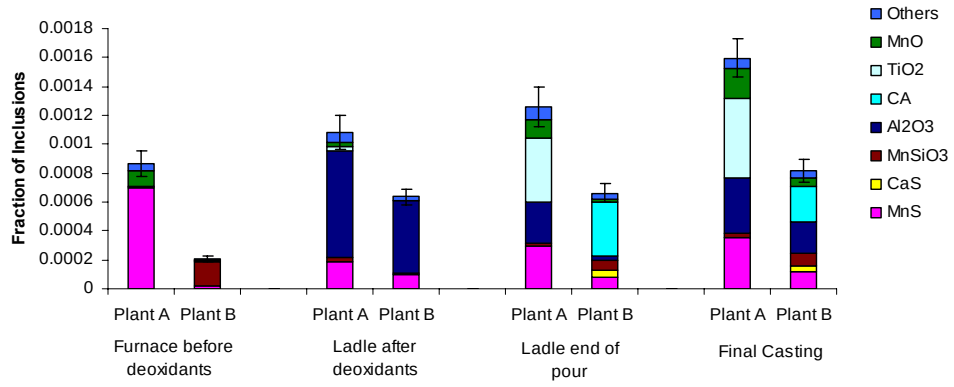

a)

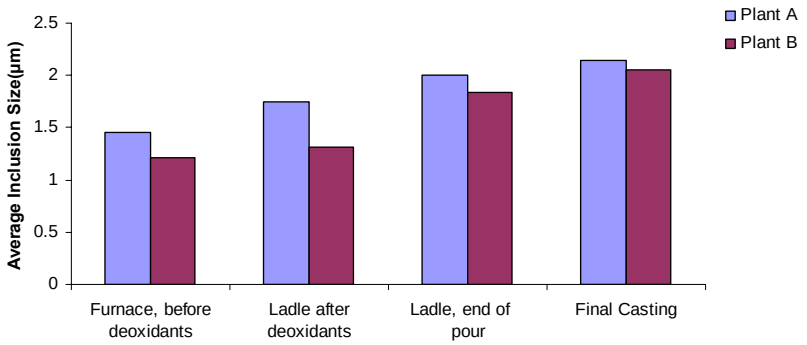

b)

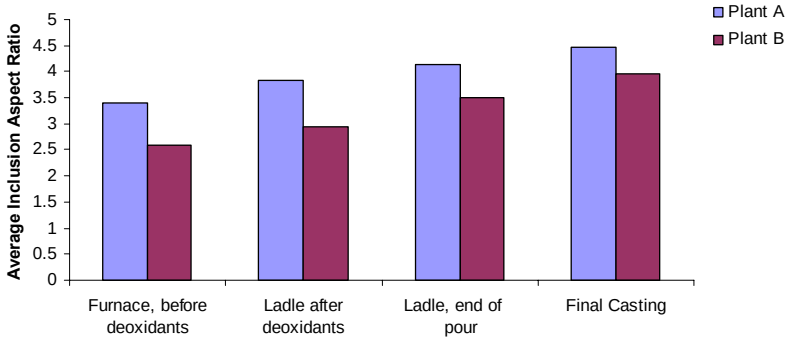

c)

Figure 2.16. Comparison of inclusion a) volume, b) size and c) aspect ratio measured in samples collected at various stages of the casting process, for plant A with no calcium-treatment and plant B with CaSi added during tap

2.3.5.2. Effect of acid versus basic practice. Figure 2.17 compares the samples collected from the 20 ton acid and basic EAFs, at the same foundry. Both had similar

ladle-size and ladle-practices, except more calcium was added in the acid practice in the ladle than the basic practice. The basic practice did not have as many sulfide inclusions as the acid practice. Ca-treatment in the acid practice was more effective than the basic practice in reducing the MnS and alumina inclusions, but the basic practice had fewer inclusions in the cast sample. Ca-added in the basic process was not sufficient and it did not cause any appreciable modification or reduction of alumina or MnS inclusions (Figure 2.17 a).

The inclusions in the acid practice were found to be smaller and more round than the basic practice. This was due to the better Ca-treatment performed in the acid practice. But in this case also, reoxidation decreases the difference between the two practices in terms of their shape and size (Figure 2.17 b and c).

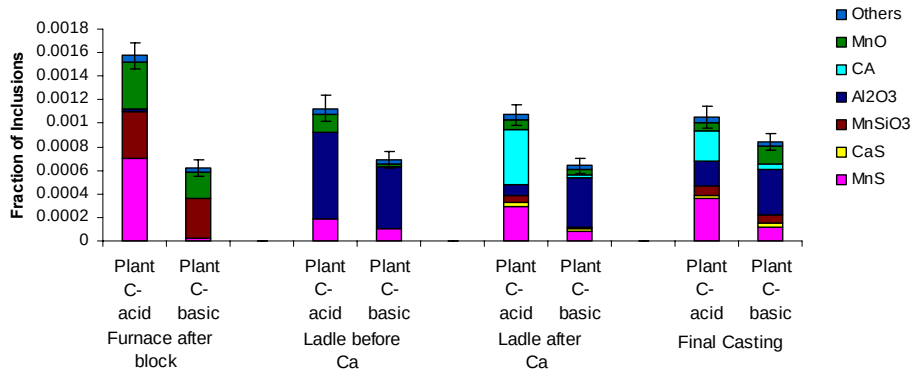

a)

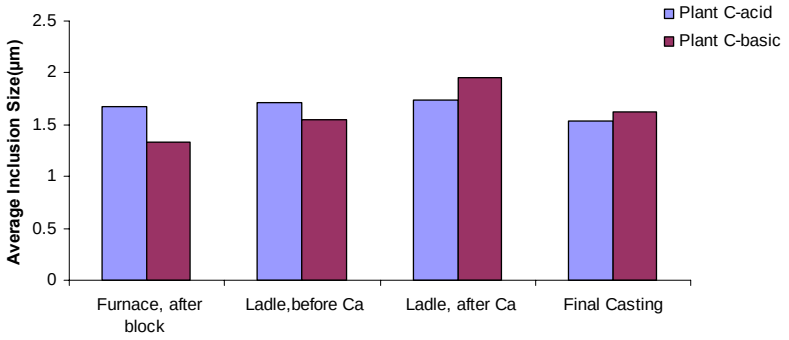

b)

Figure 2.17. Comparison of inclusion a) volume, b) size and c) aspect ratio measured in samples collected at various stages of the casting process, for plant C acid and basic practice

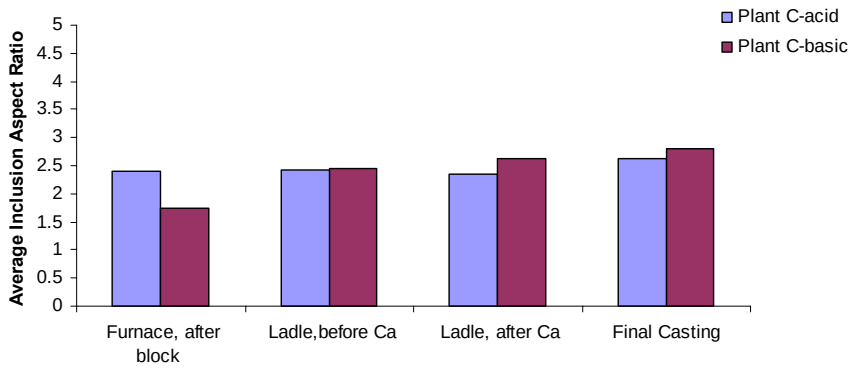

c)

Figure 2.17. Comparison of inclusion a) volume, b) size and c) aspect ratio measured in samples collected at various stages of the casting process, for plant C acid and basic practice (cont.)

2.3.5.3. Effect of inclusion spacing. Apart from the inclusions shape, size, number and composition, one more property affects the cleanliness and properties of steel, which is the average spacing between the inclusions. As discussed in equation (2) in Section 1.2, the fracture toughness of steel is directly proportional to the spacing between the inclusions. So, "clean" steel should have widely spaced inclusions in order to achieve high toughness [9].

Aspex measures the exact coordinates of the inclusions on the microscopic specimen. In order to measure the spacing between the inclusions through Aspex, all the coordinates of the inclusions were exported to a Microsoft Excel file. After enabling the macros in Excel, a code was written using Visual Basic to calculate the distance from each inclusion to the other inclusions and determine the distance to the closest neighbor. These distances are averaged over all inclusions to determine the average spacing between the inclusions in the specimen. The complete Visual Basic code is given in Appendix B.

Figure 2.18 compares the a) area fraction covered by inclusions and b) the average spacing between the inclusions in the final cast product from all the plants. It can be seen that the spacing between the inclusions is indirectly proportional to the volume of inclusions. This implies that in cleaner samples, not only do the inclusions occupy less

volume but they are also more spread out. Hence, the "cleanest" castings not only have the least number of inclusions, but a smaller inclusion volume and greater inclusion spacing.

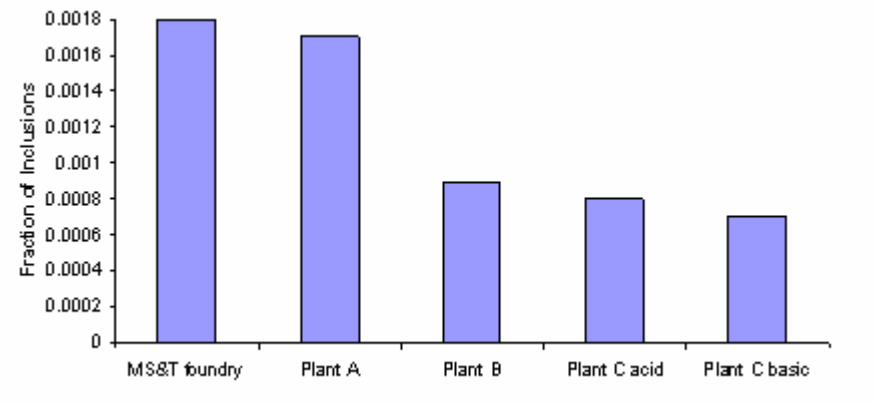

a)

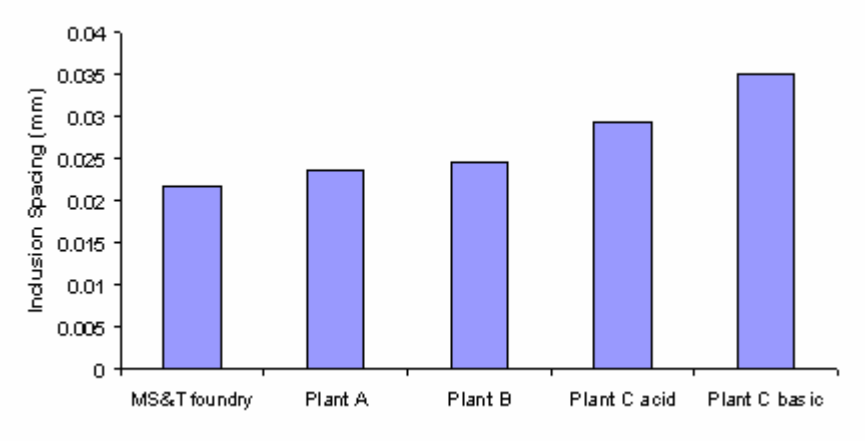

b)

Figure 2.18. Comparison of a) inclusion volume, b) average inclusion spacing in the samples from cast products collected from the different plants

2.3.5.4. Effect of ladle size. As seen from Figure 2.18 a), the inclusion content in the casting also varies with the size of the ladle. It is easier to float out inclusions from larger ladles [2]. The ladle treatment in the MS&T foundry and Plant B was similar, but Plant B had lesser inclusions because its ladle was almost 10 times the size of the MS&T foundry ladle, thus, facilitating inclusion floatation.

3. FLUENT MODELING

In this study, inclusion flotation in industrial foundry ladles was modeled using FLUENT CFD Version 6.3.26. The computational procedure included solving the equations for: 1) unsteady heat transfer between the molten steel and the ladle lining, 2) free convection flow of the molten steel as a result of the changing steel density, and 3) particle flow in the liquid steel by applying drag forces.

The unsteady heat transfer was solved by using a "coupled" thermal boundary between the liquid steel (1600°C) and the preheated ladle lining (900°C), and assuming that there was radiation and convection from the open steel surface at the top. The free convection flow of the steel was solved using the Boussinesq density model for thermally expanded liquids [27].

Figure 3.1 shows the ladle design used for modeling the flow of the steel. The ladle design consists of two concentric cylinders, with a refractory lining in between. Table 3.1 gives the dimensions of the ladle, which were varied to provide different ladle sizes. The density of the liquid steel was taken to be 7000 kg/m^3, according to the Boussinesq density model [27].

Table 3.1. Dimensions of the theoretical ladles used for the different ladle sizes

Inner H (m)	Inner D (m)	Volume (cubic m)	Outer H (m)	Outer D (m)	Thickness (inch)	Mass (kg)
0.35	0.18	0.01	0.36	0.20	0.50	58.90
0.50	0.35	0.05	0.53	0.40	1.00	336.57
1.00	0.70	0.38	1.05	0.80	2.00	2692.55
1.50	1.05	1.30	1.58	1.20	3.00	9087.36

In order to introduce inclusions into the liquid steel, particles were injected randomly into the metal during each step of solving the energy and flow equations. The specific drag forces were applied on the particles, assuming that they were either spherical, non-spherical with a shape factor of 3.0 or in the form of a second phase liquid

droplet. In the case of liquid droplets, the possibility of collision and coalescence of droplets was also taken into account. It was assumed that the injected particles were reflected back into the metal from the bottom of the ladle, but that the particles escaped on reaching the top or the sides of the metal surface. The flotation of both the mono-sized and the multiple-sized particles was modeled, using the Rosin-Rammler distribution [28]. For all of the calculations, the density of the inclusions was assumed to be 2.7 g/cc and the non-spherical particles were assumed to have a shape factor of 3.0, based on a reference found in the literature [29]. The largest ladle size of 9100 kg was chosen for all the modeling calculations as this size was mid-way between the large and the small ladles studied in this research.

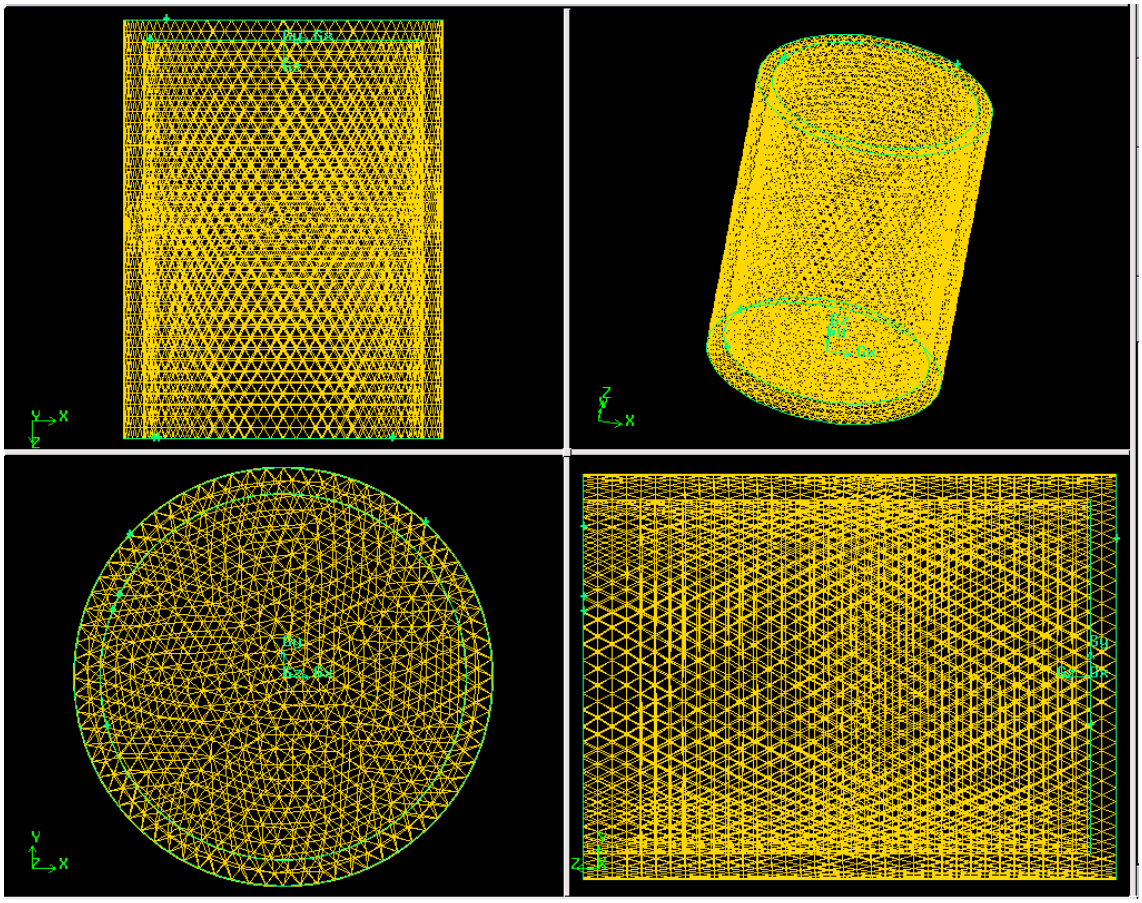

Figure 3.1. Ladle design used for modeling the flow of the liquid steel

3.1. DIFFERENT FLOW MODELS

The flotation of spherical inclusions of different sizes by gravity forces alone and by natural convection is compared in Figure 3.2. It can be observed that although the large spherical particles escape in approximately the same time for both the cases, micron-sizes particles were not floated out by gravity, but were partially removed from the liquid metal by natural convection.

A more intensive flow of the molten metal than natural convection helps in improving steel cleanliness. One of the possible ways of increasing the metal flow rate is adding Ar-stirring in the ladle. Figure 3.3 shows the particle motion of spherical inclusions of size 50 μm in a 9100 kg capacity ladle in the presence of Ar-stirring at the bottom. The porous-plug is at the centre of the bottom of the ladle and the rate of Ar-flow is 3.5 cfm. It can be seen that most of the particles escaped the ladle at the end of 60 seconds in the presence of Ar-stirring.

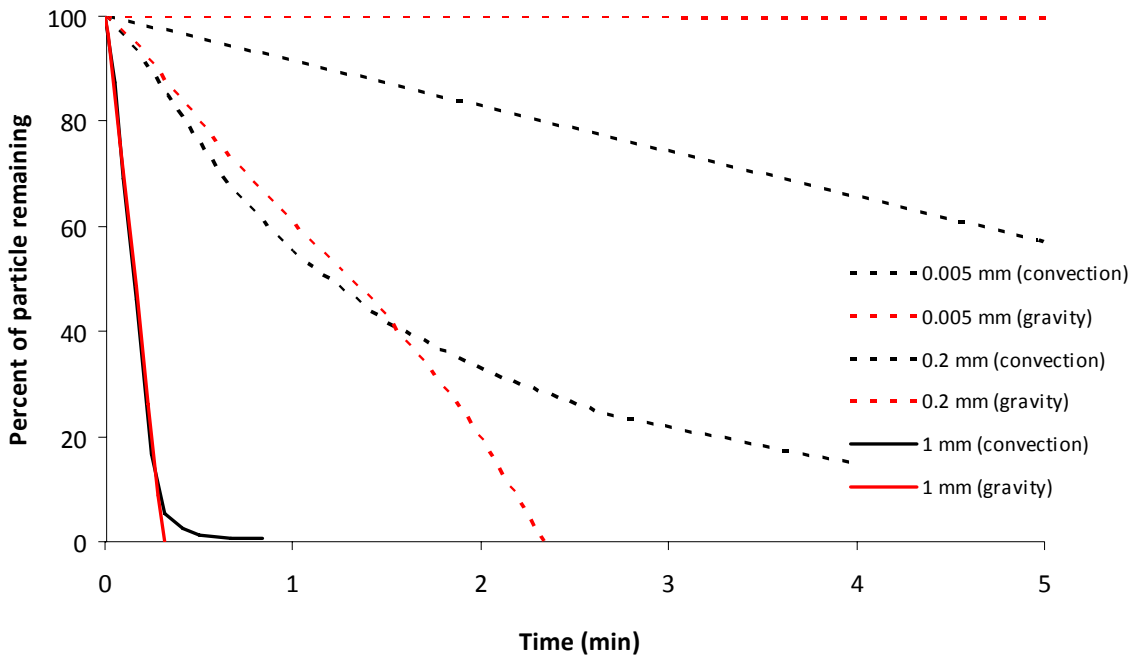

Figure 3.2. Effects of gravity and natural convection on inclusion escape from the liquid steel

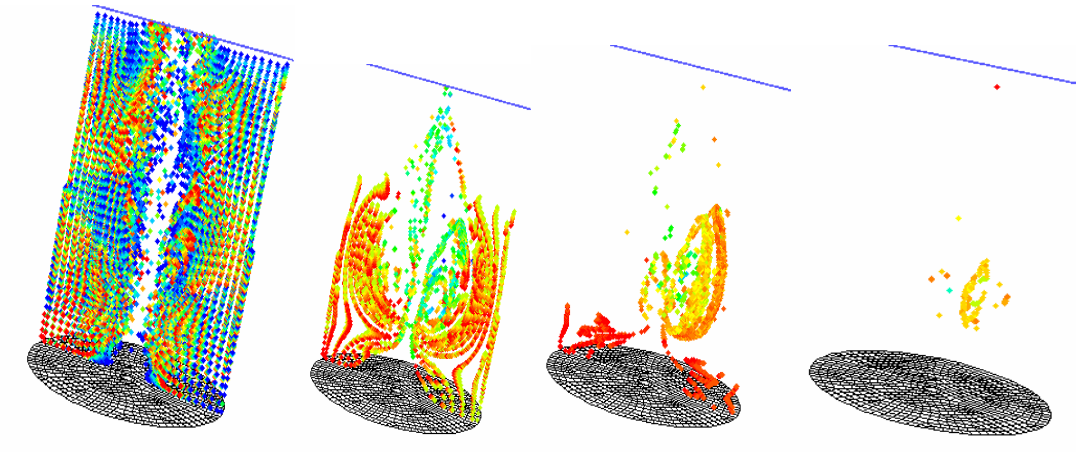

1 sec 4 sec 20 sec 60 sec

Figure 3.3. Flow of spherical particles of size 50 μm in a 9100 kg ladle with Ar-stirring at the bottom of the ladle through a porous plug

3.2. EFFECT OF LADLE SIZE

The flotation of the injected spherical particles in the molten metal, in the presence of only natural convection, for different ladle capacities is shown in Figure 3.4. It was interesting to observe that ladle size had a negligible effect on particle flotation in the model. The larger ladles had longer flotation distances compared to the smaller ladle, but more intensive convection, thus reducing the flotation time. Because of these two factors, the hold-time of the molten steel in the ladle is the main factor limiting inclusion flotation. The typical hold-time in minutes for the different ladles is shown with red arrows in Figure 3.4.

3.3. EFFECT OF INCLUSION SHAPE AND SIZE

Figure 3.5 shows the dependence of particle flotation on its size, for spherical particles, in the presence of natural convection in the molten metal. The larger particles were observed to float out and escape faster as compared to the smaller ones. This explains the flotation of larger Al_2O_3 inclusions, whereas the smaller TiO_2 inclusions remained in the steel, as observed in Section 2.3.1.

Figure 3.6 shows the effect of the inclusion shape factor and density on inclusion flotation, in the presence of natural convection in the metal. Four different kinds of

particles were studied: 1) spherical particles with density 2.7 g/cc, 2) non-spherical particles with density 2.7 g/cc and shape factor 3.0, 3) spherical particles with density 1.7 g/cc, and 4) coalesced liquid droplets with density 2.7 g/cc. It can be seen that the less dense particles float faster than the dense particles. The non-spherical particles were found to float faster than the spherical ones. This can be explained because in this case it was assumed that only natural convection is acting on the particles and the drag force, which is more on the non-spherical particles, is helping the particles float out. Also, the coalesced liquid droplets have the highest flotation rate. This observation helps in explaining the reduction in inclusions by Ca-treatment, because calcium modifies the inclusion morphology with partial transformation of solid particles to liquid droplets allowing for more rapid escape.

The green line shows the formation of liquid droplets through coalescence with time. The increase in the number of liquid droplets with time, as shown on the y-axis on the right, shows that the possibility of droplet collision and coalescence increases with time.

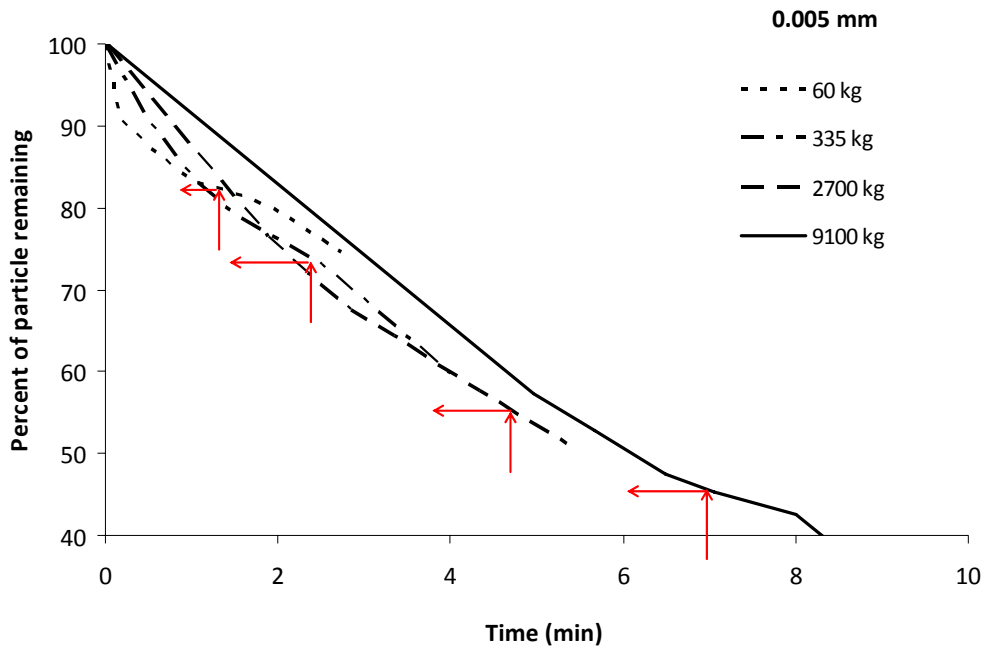

Figure 3.4. Calculated rate of inclusion flotation in the ladle with natural convection, with the red arrows showing the typical molten steel hold-time for the different ladles

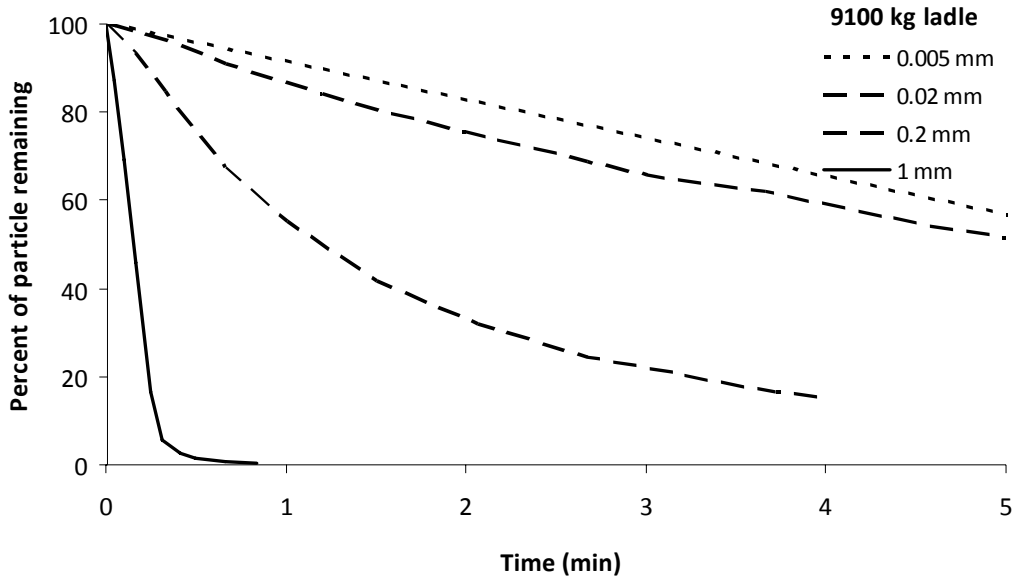

Figure 3.5. Effect of the size of spherical particles on the particle escape-rate in the presence of natural convection

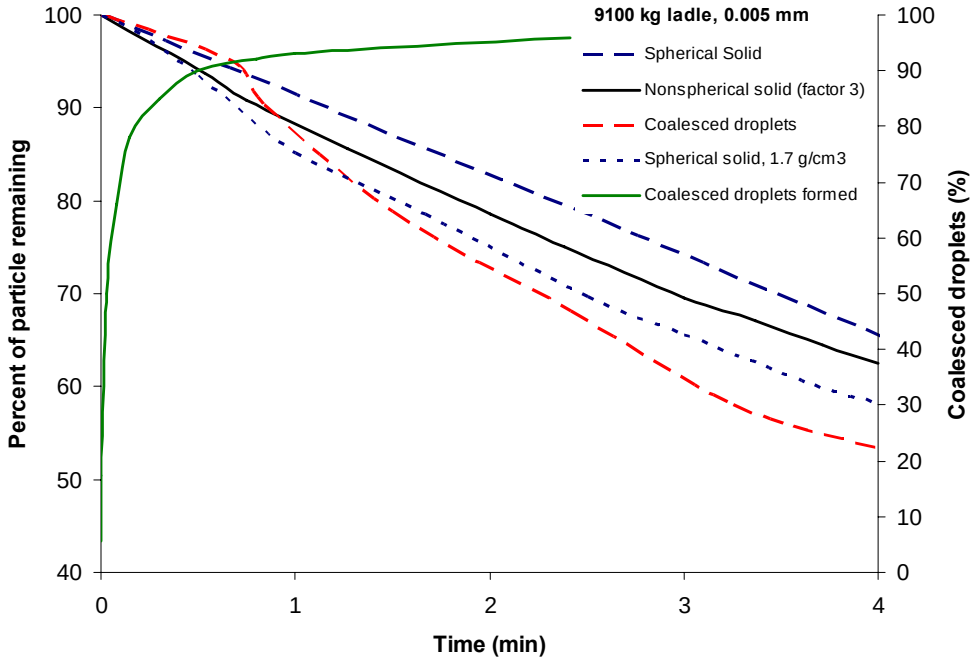

Figure 3.6. Effect of the particle shape, density and state on the inclusion escape-rate from the molten steel in the ladle, and the formation of coalesced liquid droplets, in the presence of natural convection

4. CALCIUM TREATMENT TRIALS

In the previous trials, steel cleanliness was found to be dependent on the amount and type of the deoxidants added. Ca deoxidation was found to be beneficial when added as wire and in sufficient quantities. It modified MnS to CaS with globular morphology, which is less harmful to mechanical properties of steel. Ca also transformed alumina to calcium aluminates (CA) with lower melting point and spherical morphology allowing them to easily float out, resulting in cleaner steel. Also, Ca-additions in the form of wire injection gave better results than bulk additions in the ladle.

In order to study the effect of Ca-addition in detail, more trials were conducted at Plant A. In these trials, different amounts Ca-wire and CaSi-wire were injected in the ladle with a wire-feeder. Ar-stirring through a pipe was also performed in the ladle in some of the heats along with Ca-addition to evaluate its effect on inclusion flotation and removal.

4.1. EXPERIMENTAL PROCEDURE

Five heats were studied at an industrial foundry to determine the effects of Ca-wire and Ar-stirring on inclusions in medium carbon cast steel. Steel was melted in a medium frequency induction furnace (IF) of 2200 lbs capacity, equipped with a porous plug at the bottom, and tapped twice into a 1000 lbs ladle.

4.1.1. Regular Practice. The regular practice at the foundry included a 10 minute Ar-stir in the IF, at a pressure of 25 psi and flow-rate of 2 cfm, and deoxidation in the furnace with 1 lb Al and standard FeMn and FeSi block additions. This was followed by a treatment of 1 lb of Al, 0.66 lbs of Fe70Ti alloy and 0.88 lbs of Fe51Si35Zr alloy into the ladle, during tap.

4.1.2. Post-tap Treatment. In the trials conducted, the post-tap treatments in the ladle were varied for the different heats. The different treatments were planned to observe the effect of the following parameters on the inclusions and the oxygen content:

1) CaSi wire addition, with the wt. % of Ca added varied from 0.02 % to 0.06 %
2) Pure Ca-wire addition

3) CaSi-wire addition at high speed

4) Ar-stirring with lance in the ladle for 1 min.

5) Combined Ar-stirring and CaSi-wire addition

The post-tap treatment for each of the two ladles in each heat is summarized in Table 4.1.

Table 4.1. Post-tap treatment of each ladle in all of the heats

Heat	Ladle	Post-tap Treatment
A	1	No post-tap treatment
	2	CaSi wire addition in the ladle. 0.024 wt. % of Ca added at a wire feed-rate of 12.5 ft./minute.
B	1	CaSi wire addition in the ladle. 0.028 wt. % of Ca added at a wire feed-rate of 12.5 ft./minute
	2	Pure Ca wire addition in the ladle. 0.032 wt. % of Ca added at a wire feed-rate of 12.5 ft./minute
C	1	CaSi wire addition in the ladle. 0.043 wt. % of Ca added at a wire feed-rate of 12.5 ft./minute
	2	CaSi wire addition in the ladle. 0.05 wt. % of Ca added at a wire feed-rate of 12.5 ft./minute
D	1	CaSi wire addition in the ladle 0.043 wt. % of Ca added at a wire feed-rate of 12.5 ft./minute + Ar-stirring in ladle for 1 minute
	2	High speed CaSi wire addition in the ladle. 0.06 wt. % of Ca added at a wire feed-rate of 20 ft. /minute
E	1	No Ca-addition + Ar-stirring in ladle for 1 minute

The specifications of the pure Ca-wire and the CaSi-wire used in the trials are as given below:

1) Ca wire (Ca = 98.5%, Al =0.5%, Mg=0.5%) [Diameter =9 mm] (Weight of Ca-wire/ft=0.034 lbs/ft; weight of Ca/ft =0.0335 lbs/ft)

2) CaSi wire (Ca = 28-32%, Al =1.5%, Si=58-62%, C=1%, Fe=5%) [Diameter =9 mm]
(Weight of CaSi-wire/ft= 0.070 lbs/ft; weight of Ca/ft = 0.021 lbs/ft)

The Ar-stirring was done in the ladle of depth 24 inches for 1 minute, using a submerged lance at the pressure of 45 psi and flow-rate of 3.5 cfm.

4.1.3. Speed of Wire-Injection. Figure 4.1 shows a picture of the wire-feeder with the attached feeding-tubes. The five ft. long feeding tube was used for all the trials as it provided a safe distance between the wire-feeder and the hot metal. A speed of 12.5 ft/min was used in most of the heats for wire-injection. A higher speed of 20 ft/minute was tried for one of the heats, to obtain deeper injection of the wire in the liquid steel but resulted in an electrical circuit failure. Therefore, only one heat used the higher speed of wire-injection.

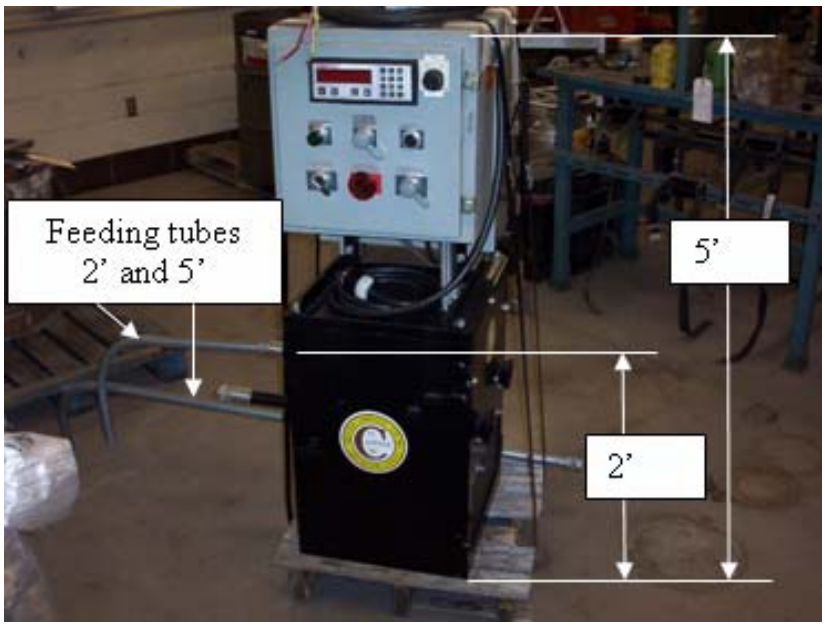

Figure 4.1. Picture of the wire-feeder with the feeding tubes

4.1.4. Sampling and Oxygen Measurement. Steel chemistry samples were collected from the furnace, ladle and the mold, using submerged chemistry samplers (SaF 400-QS 3012 from Heraeus Electro-Nite). The samples were collected before and after deoxidation and post-tap treatment. In addition, samples were cut from standard keel

blocks cast from the same heat. Microscopic specimens were prepared from these samples and a 10 mm^2 area was analyzed in each specimen for inclusions using the Aspex PICA-1020 for automated inclusion analysis. The total oxygen content was measured from all the samples collected, using Leco TC-500. The dissolved oxygen content was measured directly from the liquid steel, through all the stages of the casting process, using Celox oxygen probes and the Celox Lab Datacast-2000.

4.2. RESULTS AND DISCUSSION

4.2.1. Standard Practice. One regular ladle pour was followed during the trials, with no additional post-tap treatment. Figures 4.2 compares the a) area fraction covered by inclusions, b) total and dissolved oxygen, c) average inclusions size and d) average inclusion aspect ratio, at the various stages of liquid processing.

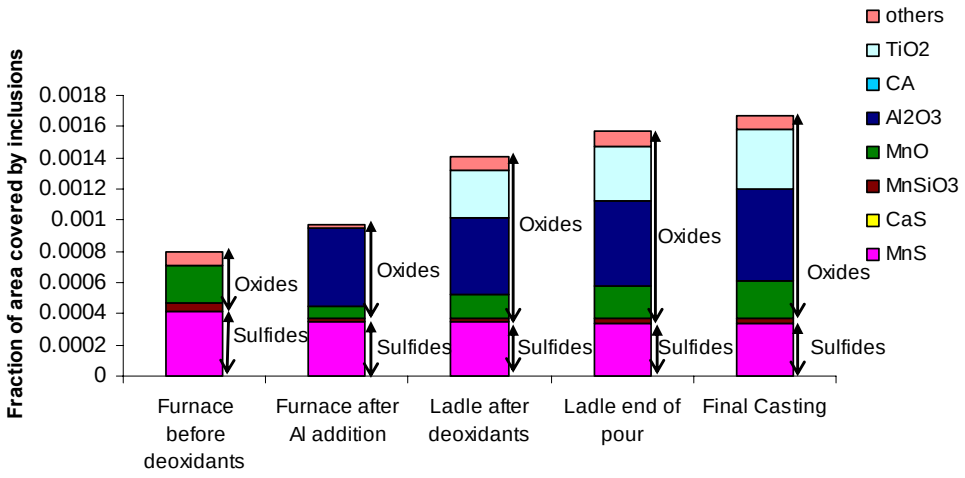

a)

Figure 4.2. Comparison of a) inclusion volume, b) dissolved and total oxygen, c) average inclusion size, and d) average inclusion aspect ratio measured in samples collected at various stages of the casting process, standard practice, no post-treatment

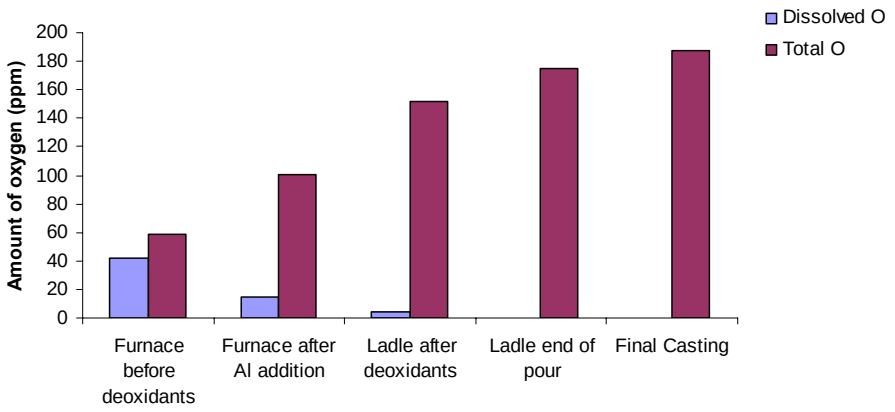

b)

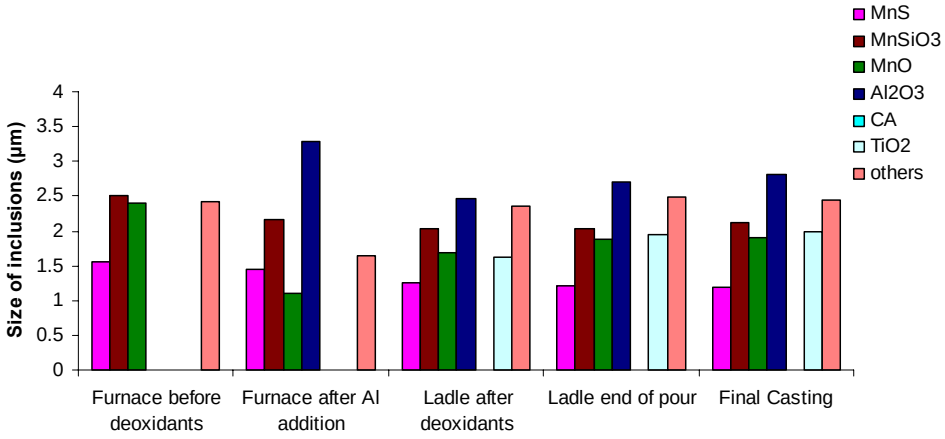

c)

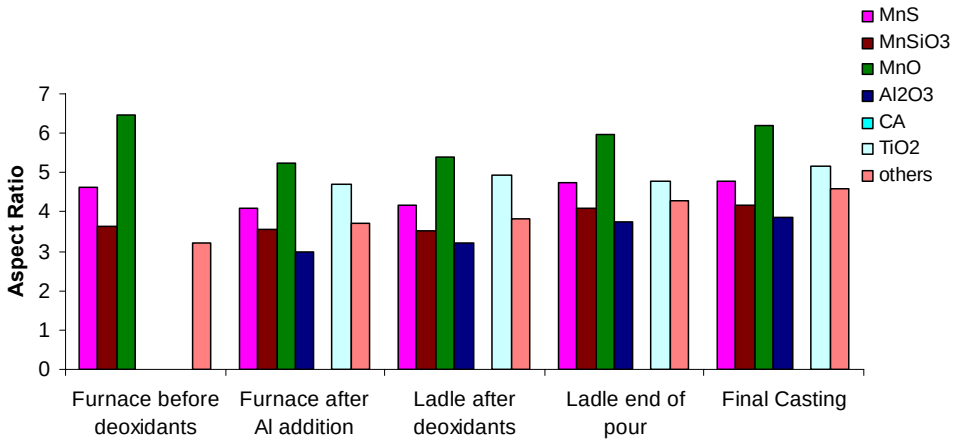

d)

Figure 4.2. Comparison of a) inclusion volume, b) dissolved and total oxygen, c) average inclusion size, and d) average inclusion aspect ratio measured in samples collected at various stages of the casting process, standard practice, no post-treatment (cont.)

The area of Al_2O_3 and TiO_2 inclusions increased after the Al and FeTi additions in the ladle. Ti is added to the cast steel as it is a stable nitride former and helps in preventing the AlN embrittlement. TiO_2 inclusions are difficult to float out due to their non-spherical shape and small size as compared to the agglomerate of alumina inclusions (Figure 4.2 c and d). The average size of the TiO_2 inclusions in the samples collected was found to be 1.7 μm, while the average size of alumina inclusions was close to 2.8 μm. The smaller inclusions are more difficult to float out and this effect is explained in detail with FLUENT modeling (Figure 3.5 in Section 3.3).

The dissolved oxygen dropped after deoxidation, resulting in the formation of a large number of oxide inclusions and an increase in the total oxygen. The area of the oxide inclusions and the total oxygen increased during the pour and also the casting had more inclusions than in the ladle, suggesting that there is significant reoxidation during pouring and the liquid steel transportation (Figure 4.2 a and b).

4.2.2. Effect of Ca-treatment. After tapping, the cast steel was Ca-treated in the ladle by feeding either CaSi-wire or pure Ca-wire in the ladle. Different amounts of Ca were added in different heats. All of the results for calcium treated ladles were similar in effects but differed in totals. Therefore, for simplification, only one set of results is included in this thesis. Figures 4.3 and 4.4 illustrate the change in inclusion properties and oxygen content in the samples collected from the different stages of the casing process, in the molten steel post-treated with 0.028 wt. % Ca (CaSi-wire, 12.5 ft/min feed-rate).

After Al treatment in the furnace, there was an increase in the alumina inclusions and the total oxygen. The composition and number of inclusions changed after the CaSi treatment in the ladle with most of the alumina inclusions forming calcium aluminates (CA) and MnS inclusions getting converted to CaS inclusions. The total oxygen also dropped with Ca addition (Figure 4.3). Also, Si addition due to the injection of CaSi wire promoted the formation of $MnSiO_3$ inclusions. The $MnSiO_3$ inclusions were huge in the casting sample, indicating that they are a product of reoxidation (Figure 4.4a). The Ca-treatment was found to be beneficial because both the types of the Ca-modified inclusions, calcium aluminate and CaS, were smaller in size and more round in shape as compared to the alumina and MnS inclusions (Figure 4.4 a and b).

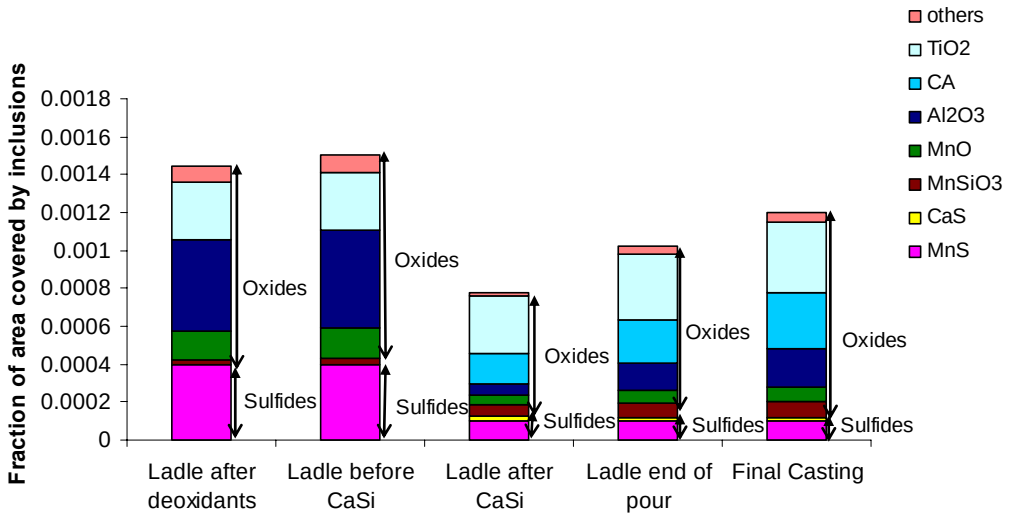

a)

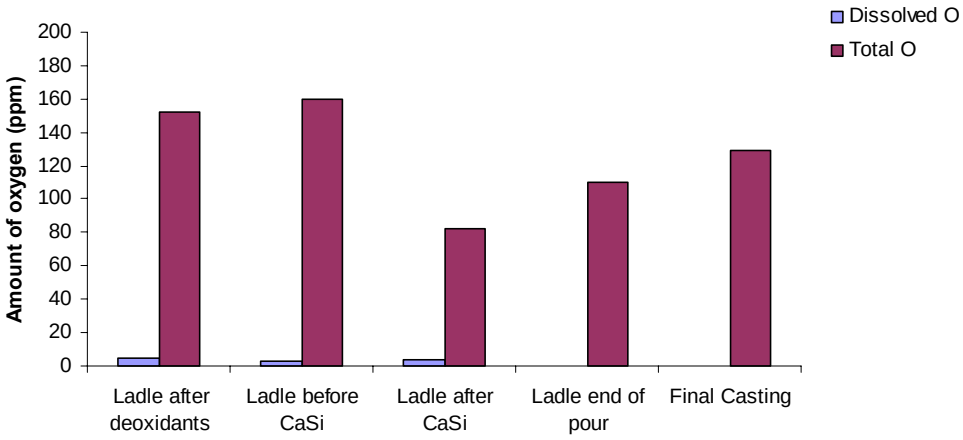

b)

Figure 4.3. Comparison of a) inclusion area and b) oxygen content measured in samples collected at various stages of the casting, post-treated with CaSi-wire, 0.028 wt. % Ca, 12.5 ft/min feed-rate

In the other ladle tests, the weight % of Ca-added was varied from 0.02% to 0.06%. The Ca-addition was made with either CaSi-wire or pure Ca-wire. No Ar-stirring was done in these heats. Figures 4.5 and 4.6 show the effect of varying the Ca-addition on the inclusions and the total oxygen content of the steel, as measured from the cast samples obtained from the various heats.

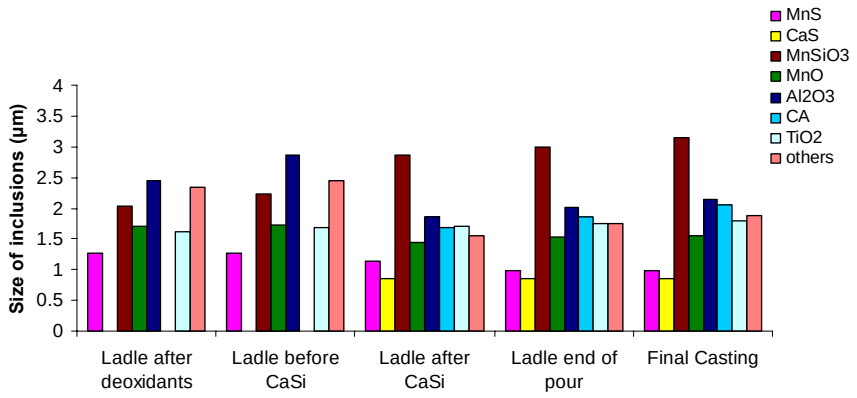

a)

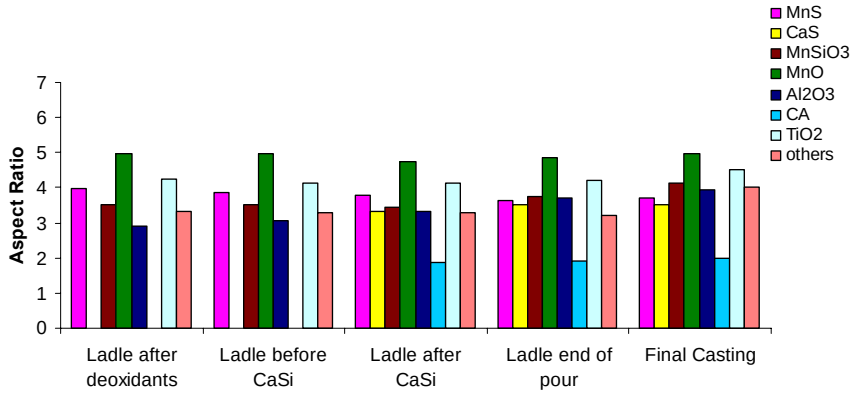

b)

Figure 4.4. Comparison of inclusion a) size and b) aspect ratio measured in samples collected at various stages of the casting, post-treated with CaSi-wire, 0.028 wt. % Ca, 12.5 ft/min feed-rate

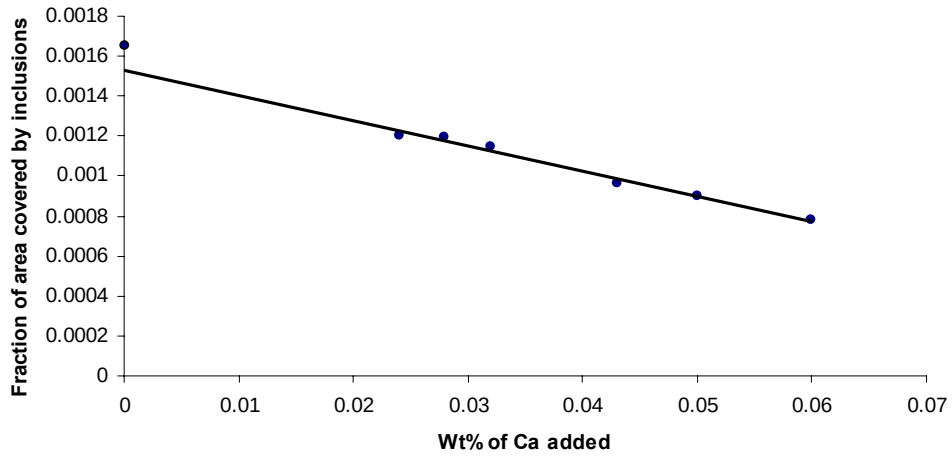

Figure 4.5. Change in the amount of inclusions with varying wt. % of Ca-addition.

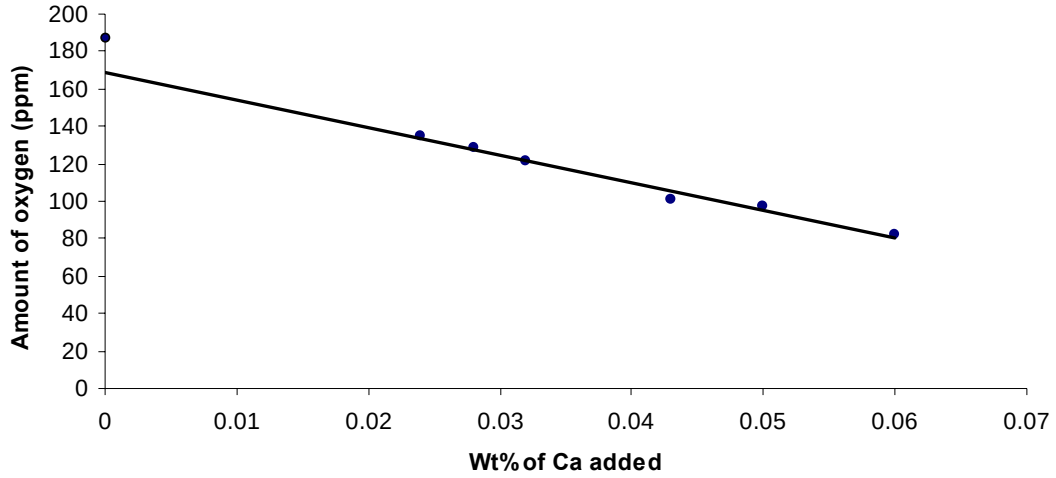

Figure 4.6. Change in the amount of total oxygen with varying wt. % of Ca-addition.

The inclusions and the total oxygen decrease, almost linearly, with increasing amounts of Ca-added. Thus, Ca-treatment gave good results in terms of improving the cleanliness of cast steel. Also, it can be observed that the actual zero point of the curve, that is, the amount of inclusions at no Ca-addition, is above the best-fit line which was projected to zero calcium. Thus, even a little amount of Ca-added helps significantly in decreasing the inclusions. This effect is proportional to the amount of calcium added. This observation is also true for total oxygen data.

Figure 4.7 shows the change in a) oxides inclusions and b) sulfide inclusions with the varying amount of Ca-added. It can be observed that both the type of inclusions decrease with Ca-addition. The graph is more linear for oxide inclusions, but there is a steeper decrease in sulfide inclusions with just a little amount of Ca. Hence, a little amount of Ca-added will decrease the sulfide inclusions first. The decrease in oxide inclusions is steady with the increasing rate of calcium addition.

The effect of Ca-addition on the shape of the inclusions is seen in Figure 4.8. The weighted average aspect ratio of the inclusions was plotted for the samples collected from a) the ladle after Ca-addition and b) the finished casting, with increasing Ca-addition in the different heats. It can be seen that the average aspect ratio significantly decreases with increasing Ca-addition in the ladle samples, showing that calcium is effective in modifying the inclusions to a spherical shape. The reduction in aspect ratio with

increasing Ca is still evident in the casting samples; however, reoxidation damaged the modification effect increasing the overall aspect ratio.

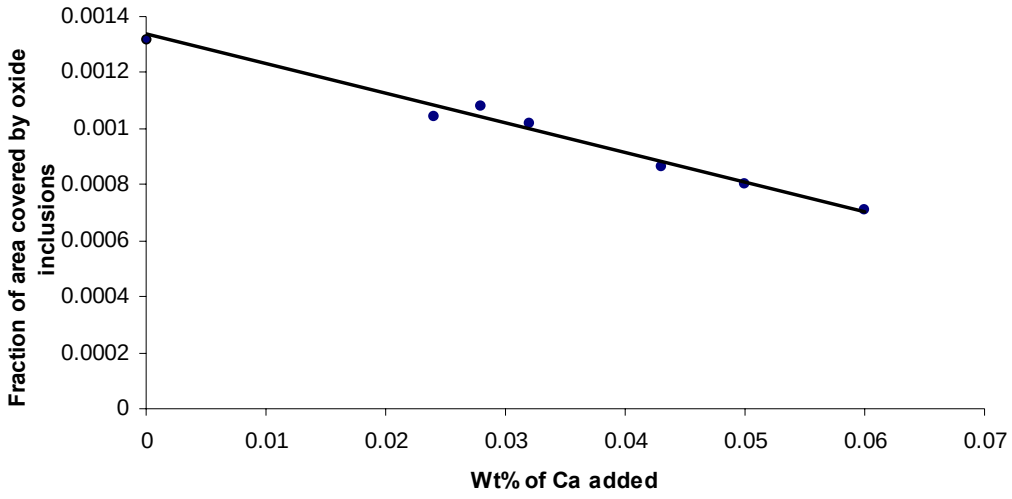

a)

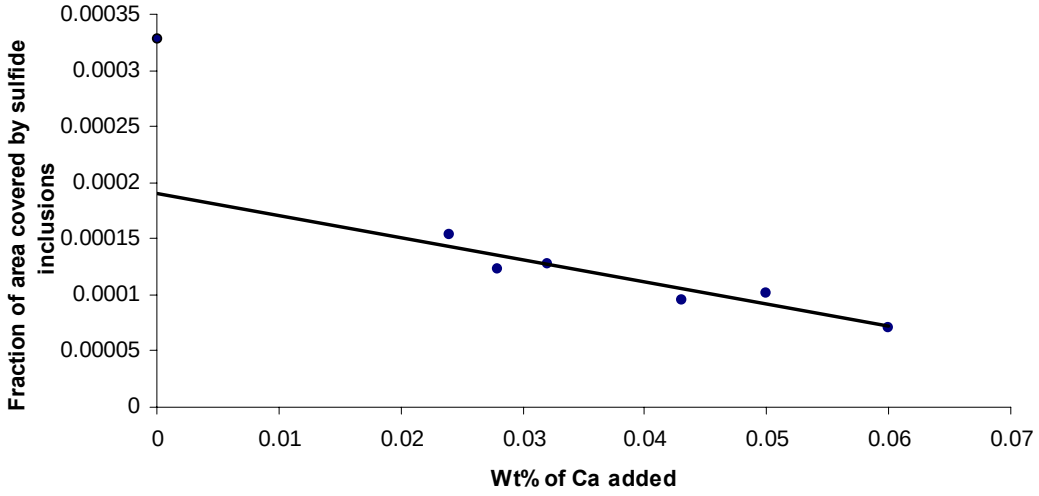

b)

Figure 4.7. Change in the amount of a) oxide inclusions and b) sulfide inclusions with varying wt. % of Ca-addition

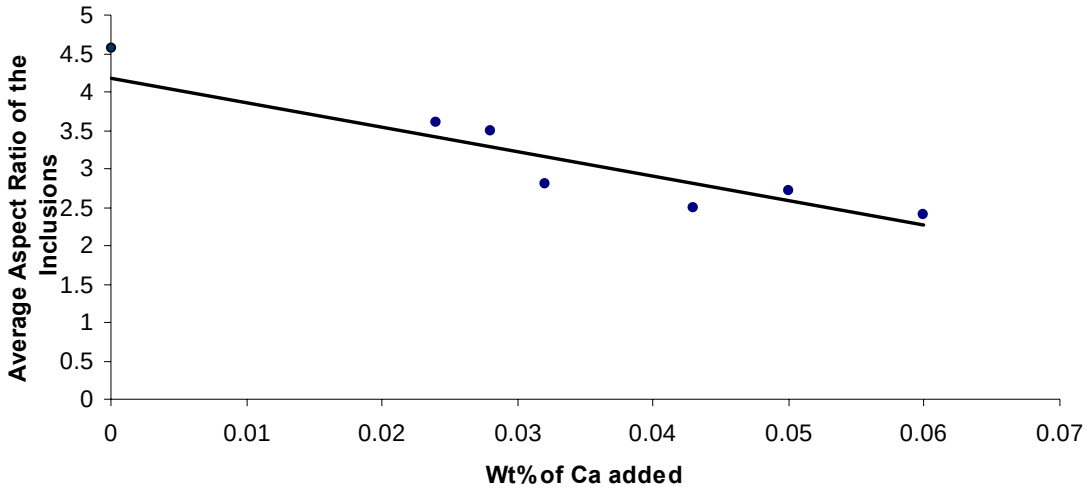

a)

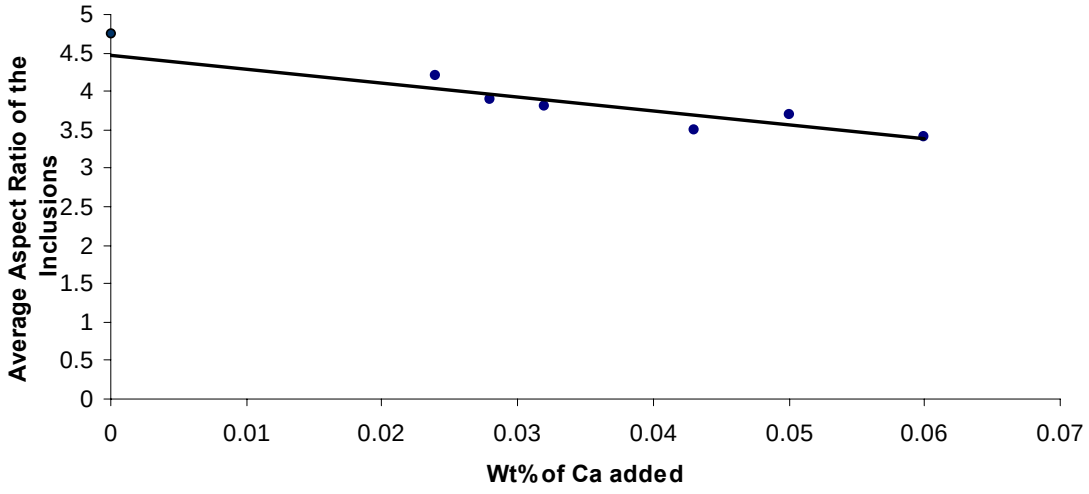

b)

Figure 4.8. Weighted average aspect ratio of the inclusions in the sample collected from a) ladle after Ca-treatment and b) casting with varying wt. % of Ca-addition in the different heats

4.2.3. Effect of Ar-stirring. In one ladle, no Ca was added in the ladle and Ar-stirring was performed with a submerged lance for 1 minute. Figures 4.9 compare the change in a) inclusions area, b) oxygen content, c) average inclusion size, and d) inclusion shape during the various stages of casting.

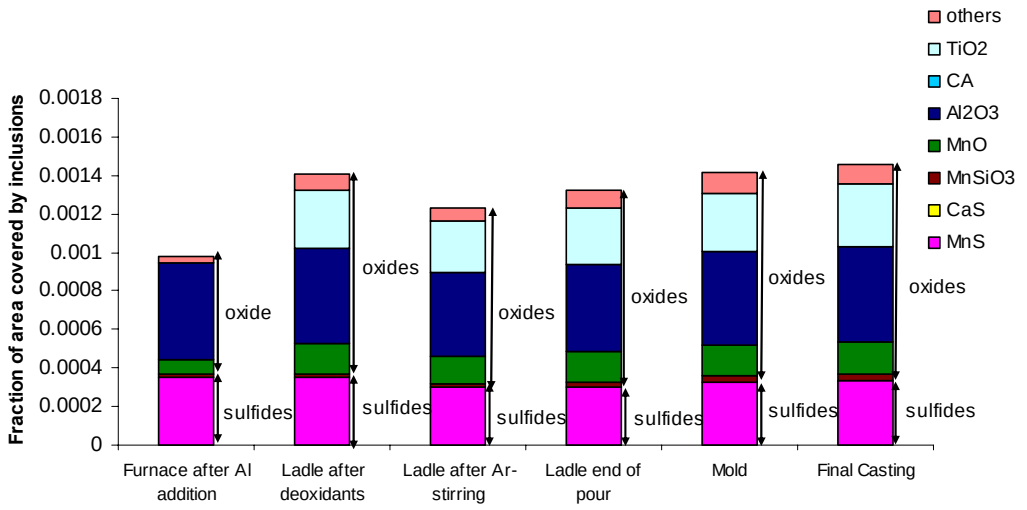

a)

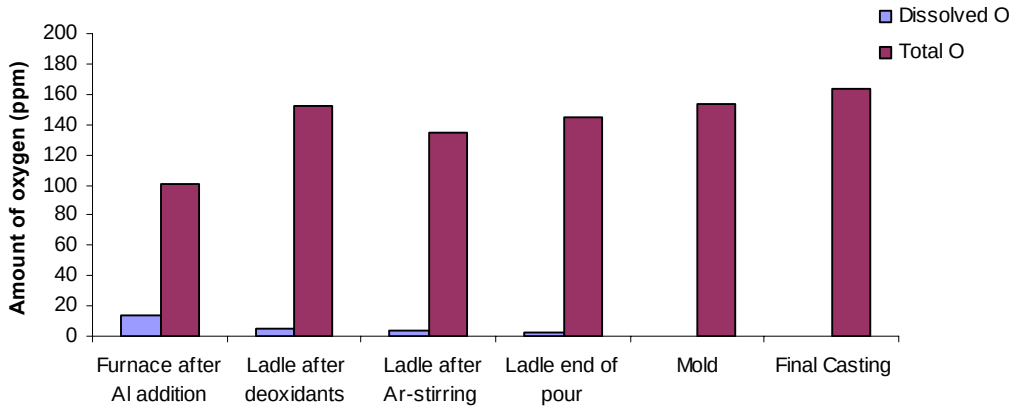

b)

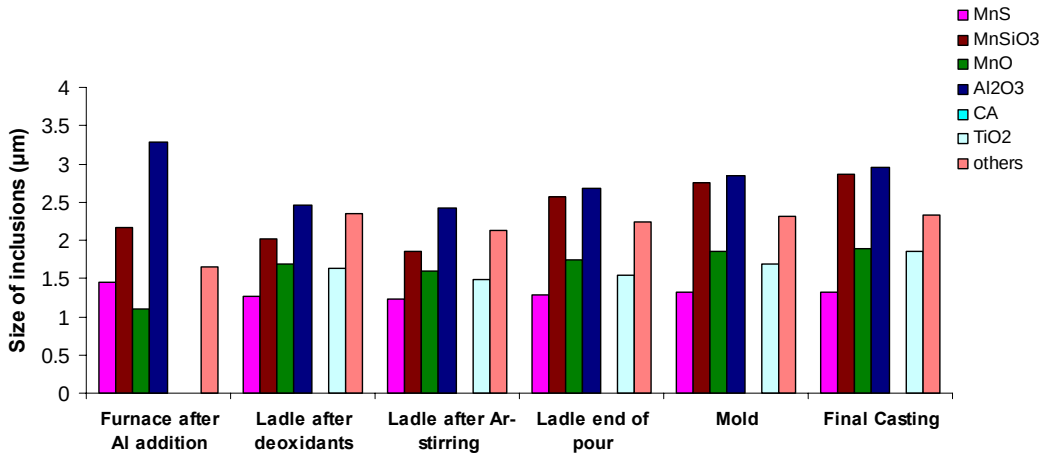

c)

Figure 4.9. Comparison of a) inclusion volume, b) dissolved and total oxygen, c) average inclusion size, and d) average inclusion aspect ratio measured in samples collected at various stages of the casting process, with only Ar-stirring in the ladle

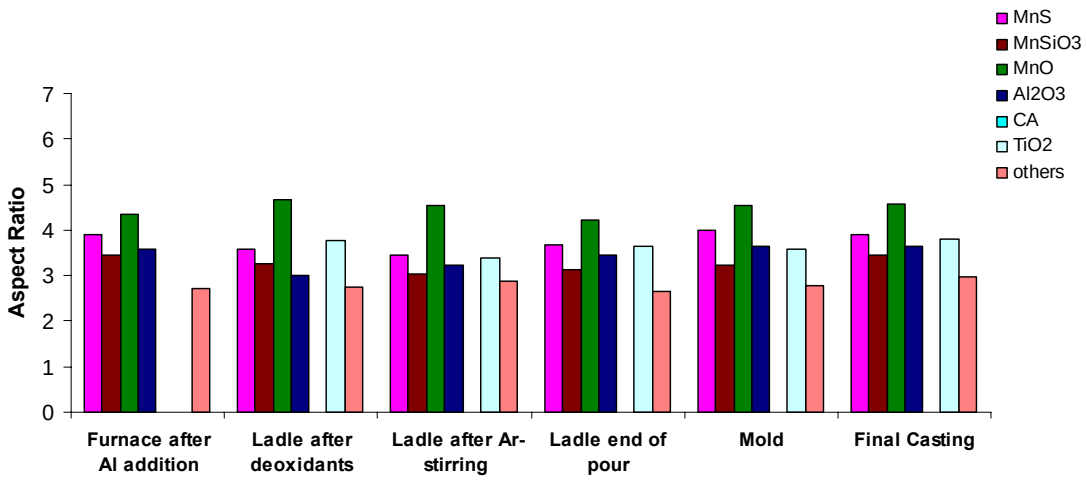

d)

Figure 4.9. Comparison of a) inclusion volume, b) dissolved and total oxygen, c) average inclusion size, and d) average inclusion aspect ratio measured in samples collected at various stages of the casting process, with only Ar-stirring in the ladle (cont.)

Ar-stirring helped with inclusion floatation. The volume of inclusions and the total oxygen decreased after the stirring (Figure 4.9 a and b). This observation is supported by FLUENT modeling discussed in Figure 3.3 in Section 3.1, which shows that an intensive flow of the molten metal caused by Ar-stirring in the ladle helps in removing almost all the inclusions at the end of 1 minute. But Ar-stirring did not cause any appreciable change in the shape or size of the inclusions, showing that Ar-stirring did not modify the inclusions, just helped them to float out (Figure 4.9 c and d).

4.2.4. Effect of Ca-addition Combined with Ar-stirring. In order to see the combined effect of Ca-addition along with Ar-stirring, and to compare these processes, a trial was conducted in which first CaSi-wire (0.043 wt. % Ca) was added in the ladle, followed by Ar-stirring for 1 minute. Figures 4.10 and 4.11 illustrate the change in inclusions and the oxygen content during the various stages of casting.

As observed in the previous cases, both Ar-stirring and Ca-addition helped in inclusion removal. The dissolved oxygen also decreased after Ar-stirring which indicates that the Ca-reaction with the liquid metal continued during the stirring. But a greater decrease in inclusions and oxygen was observed in the ladle sample immediately after

Ca-addition, as compared to the sample taken after Ar-stirring. This shows that Ar-stirring is not as effective as Ca-treatment for inclusion removal, but the combination of both Ca-addition and Ar-stirring was more beneficial for inclusion removal.

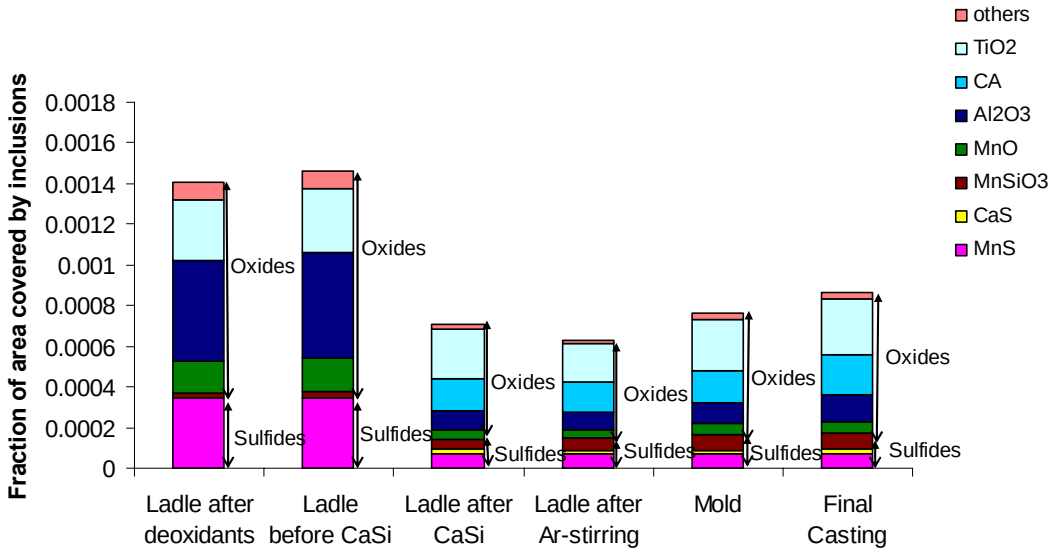

Figure 4.10. Comparison of inclusion area measured in samples collected at various stages of the casting process with CaSi-addition, 0.043 wt. % Ca and Ar-stirring in the ladle

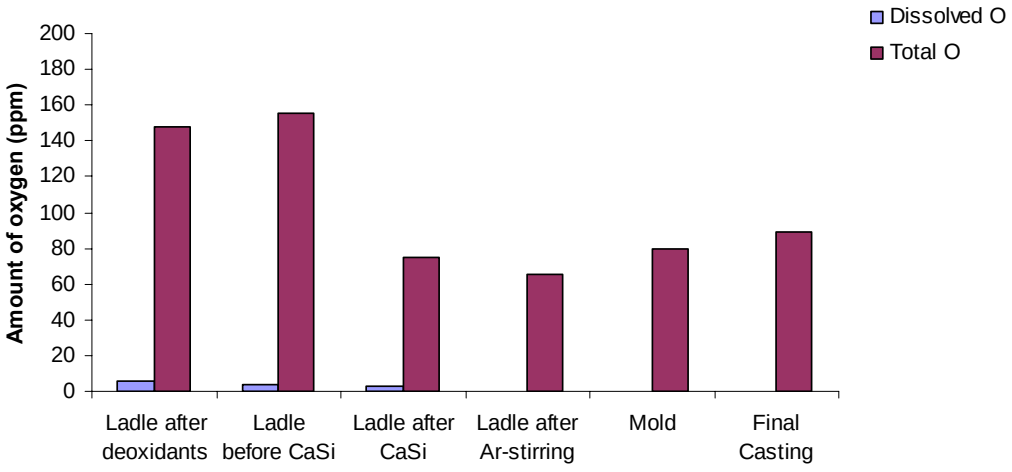

Figure 4.11. Comparison of dissolved and total oxygen at various stages of the casting process with CaSi-addition, 0.043 wt. % Ca and Ar-stirring in the ladle

4.2.5. Effect of Other Parameters. During these trials, two other parameters of Ca-addition were tested, which were high-speed injection of the wire and the use of pure Ca-wire. High speed CaSi wire addition gave better Ca-reaction with the molten steel. It also helped in decreasing the ladle-hold time, as it added more calcium for a given time due to the high speed. Pure-Ca addition also had the advantage of adding more calcium and not changing the Si-chemistry. But pure-Ca wire addition produced a violent reaction in the small ladle, thus, it was not used for any other heats.

4.2.6. Comparison of All the Treatments. The effects of the different post-tap treatments on the cleanliness and the chemistry of the cast steel are discussed here.

4.2.6.1. Effect on inclusions. CaSi-wire additions were effective in reducing the alumina and MnS inclusions and forming calcium aluminate and CaS inclusions (Figure 4.12 a). However, higher CaSi-wire additions led to an increase in $MnSiO_3$ inclusions. Better results were achieved as the amount of Ca increased. Ar-stirring in the ladle, after CaSi-wire treatment, helped in flotation and reduction of the inclusions. But Ar-stirring alone was not as effective as Ca-additions. CaSi-wire additions at a high speed gave the lowest inclusions because of the larger amount of calcium added and better interaction of the wire with the molten steel. Also, the high speed of injection helped in addition of more Ca in less time.

By definition, “clean” steel should have widely spaced inclusions in order to achieve high toughness. As discussed in Section 2.3.5.3, the spacing between the inclusions for the casting samples was measured for all the heats. It can be seen that the spacing between the inclusions is indirectly proportional to the volume of inclusions (Figure 4.12 b). This implies that in the Ca-treated heats, not only do the inclusions occupy less volume, but they are also more widely separated and, hence, represent cleaner steel.

4.2.6.2. Effect on chemistry. Table 4.2 compares the chemistry of all the heats just after the addition of the standard deoxidants during tap and chemistry of the cast products after the various post-tap treatments. This shows the effect of the respective post-tap treatment on the chemistry of the steel.

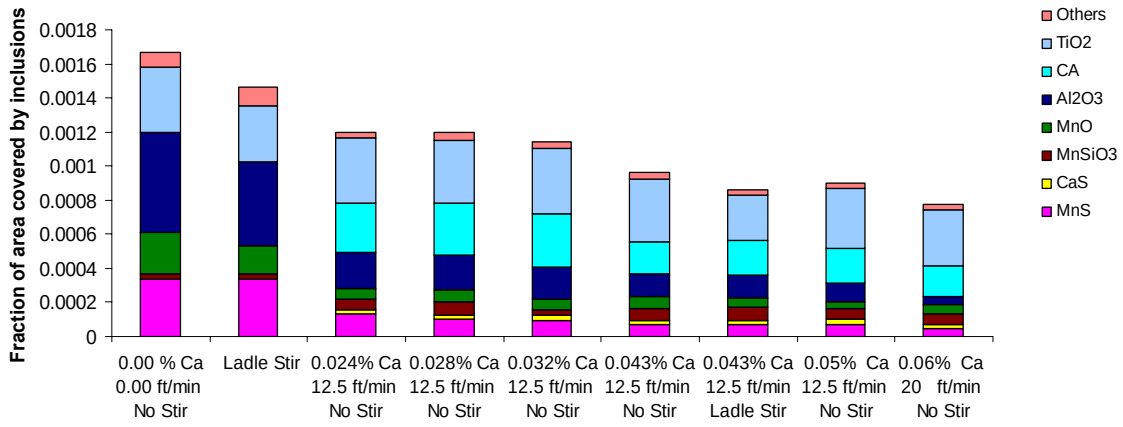

a)

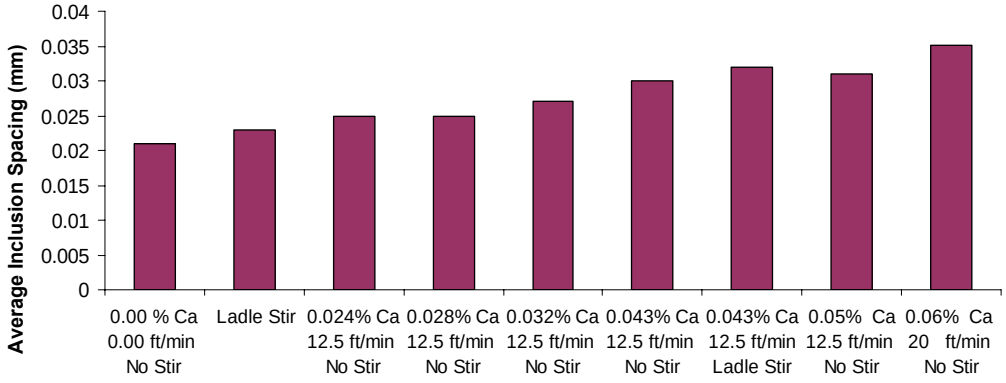

b)

Figure 4.12. Comparison of a) inclusion volume and b) average inclusion spacing in the samples taken from the cast keel blocks from all the heats

It can be seen that use of CaSi-wire increases the silicon content of the final product. But the final Si-content is below the acceptable limit of 0.05 %-0.06 %. If Si-content is above this limit, it decreases the notch-toughness of the cast product [30]. The use of pure Ca did not affect the Si-chemistry appreciably, but it caused a violent reaction in the ladle, and hence it was avoided for the other heats. The sulfur content was found to increase in the cast product, but this increase was minimized by higher Ca additions. Therefore, the Ca injection was not effective in desulfurizing due to the lack of a refining slag layer.

Table 4.2. Chemistry of some of the heats before and after the respective post-tap treatment

Treatment		C	Mn	P	S	Si	Cu	Ni	Cr	Mo	Al
CaSi-wire (0.028 wt. % Ca)	After tap	0.21	0.77	0.04	0.015	0.42	0.062	0.055	0.05	0.13	0.10
	Final	0.24	0.75	0.01	0.019	0.46	0.059	0.062	0.04	0.18	0.09
Pure Ca-wire (0.032 wt. % Ca)	After tap	0.21	0.77	0.04	0.015	0.42	0.062	0.055	0.05	0.13	0.10
	Final	0.25	0.70	0.01	0.019	0.45	0.060	0.046	0.04	0.22	0.07
CaSi-wire (0.043 wt. % Ca) + Ar-stir	After tap	0.23	0.78	0.01	0.019	0.41	0.073	0.053	0.04	0.09	0.10
	Final	0.28	0.80	0.02	0.020	0.49	0.082	0.050	0.05	0.10	0.10
No-Ca + Ar-stir	After tap	0.22	0.77	0.01	0.017	0.39	0.066	0.059	0.05	0.12	0.09
	Final	0.25	0.78	0.01	0.020	0.48	0.071	0.056	0.05	0.13	0.09

4.3. CHARPY IMPACT TESTING

4.3.1. Procedure. The cast keel blocks obtained from the heats were normalized by heating at 1650°F (900°C) for 1.5 hours and air-cooling. Charpy V-notch specimens of dimensions 10mm×10mm×55mm were prepared form the normalized keel blocks according to ASTM E23 standards [31]. The Charpy tests were conducted at a temperature of -40°C. The specimens were cooled to this temperature by keeping them in a mixture of methane and liquid nitrogen for approximately 30 minutes.

4.3.2. Results and Discussion. Figure 4.13 shows the charpy impact energy absorbed for all the heats with the different post-tap treatments. This absorbed energy is a measure of the toughness. High toughness was obtained for Ca-treated samples, and the

toughness increased with the amount of calcium. Ar-stirring also helped in increasing the toughness. Highest toughness was obtained for the combined CaSi addition with Ar-stirring.

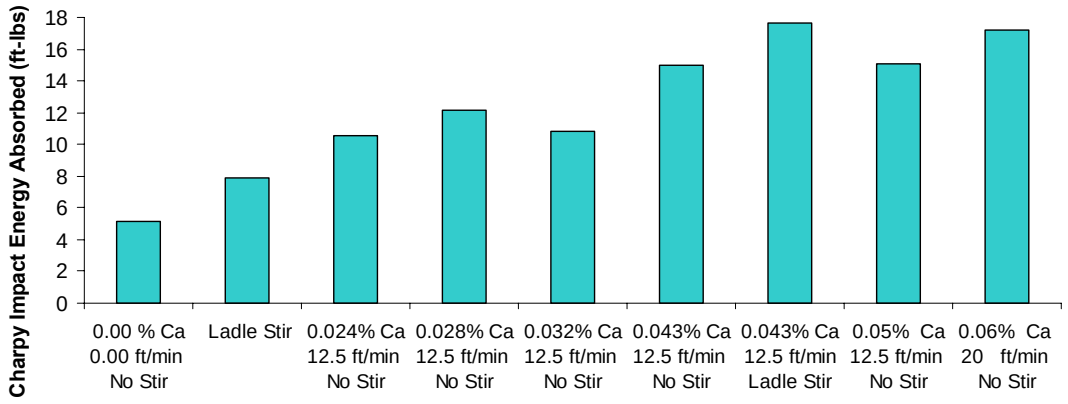

Figure 4.13. Charpy impact energy absorbed for all the different ladle treatments

Figure 4.14 shows the correlation between the toughness and the inclusions content, as measured for all the cast samples. As given in Equation 1 in Section 1.3, the fracture toughness varies linearly with $(V_f)^{-1/6}$, where V_f= volume fraction of inclusions, and assuming the rest of the parameters to be constant. The charpy impact energy data was plotted versus the (Area fraction of inclusions)$^{-1/6}$ and was observed to result in a nearly linear fit verifying this relationship. This figure directly proves that inclusions adversely affect the toughness of cast steel. For all the treatments, a decrease in inclusions has a corresponding increase in the toughness.

Figure 4.15 shows the change in the charpy impact energy absorbed with change in the (area fraction) $^{-1/6}$ of a) oxide and b) sulfide inclusions, as measured for all the cast samples. A linear relationship is observed between the toughness and the oxide inclusion fraction-$^{1/6}$, showing that decreasing the volume of oxide inclusions direct increases the toughness. The charpy impact data did not show as close of a linear relationship when plotted agains the fraction of sulfide inclusions$^{-1/6}$, but toughness definitely still increases

with a decrease in the sulfide inclusion volume. These results clearly suggest that both the types of inclusions are harmful for toughness of the cast product and should be avoided.

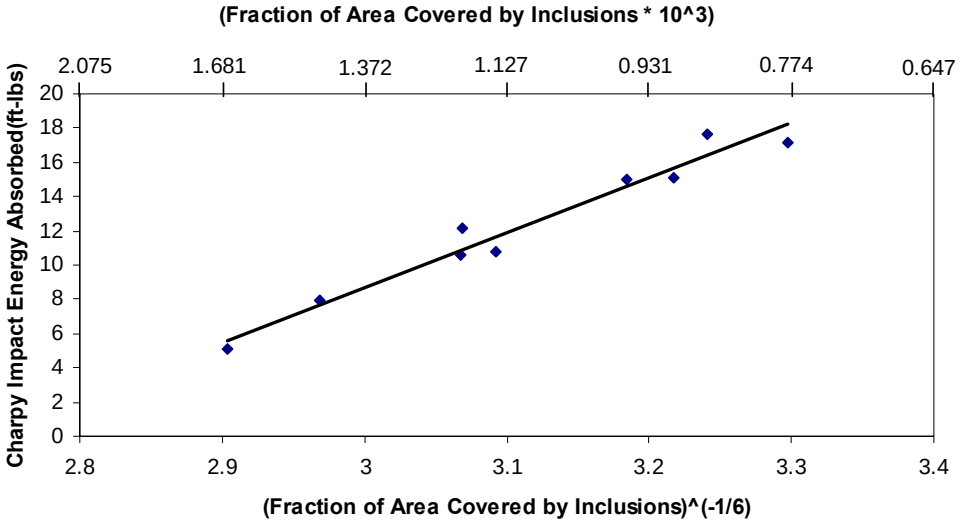

Figure 4.14. Correlation between the toughness and the inclusions content, as measured for all the cast samples

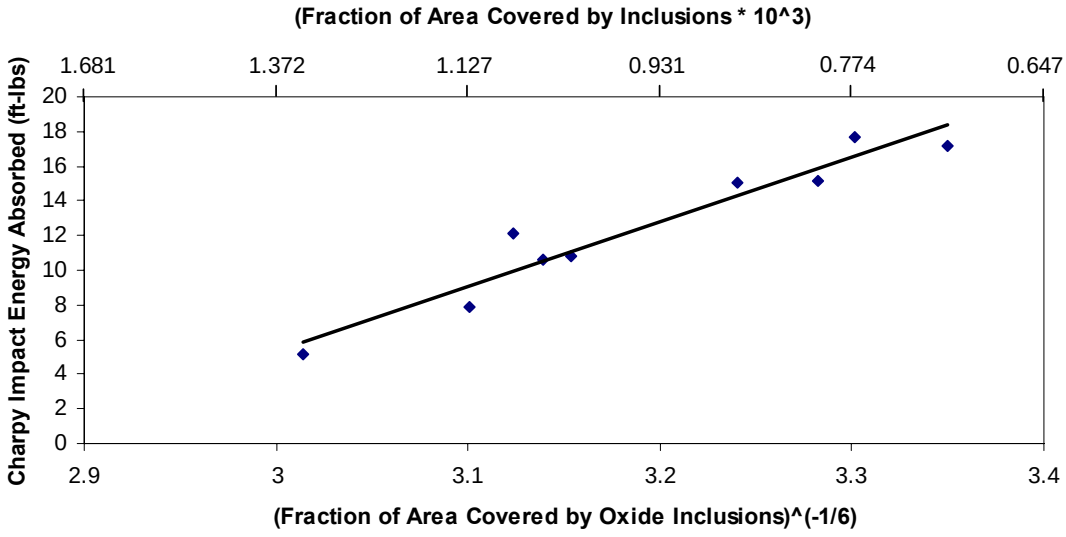

a)

Figure 4.15. Correlation between the toughness and the inclusions content for a) oxides and b) sulfides, as measured for all the cast samples

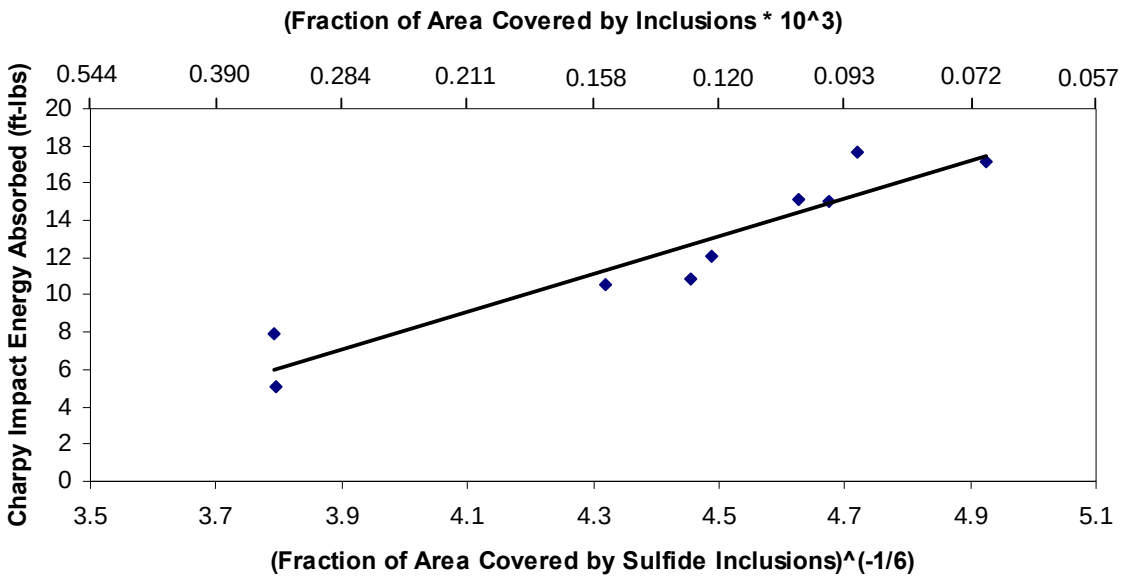

b)

Figure 4.15. Correlation between the toughness and the inclusions content for a) oxides and b) sulfides, as measured for all the cast samples (cont.)

The toughness of the casting was also found to have a direct correlation with the aspect ratio of the inclusions (Figure 4.16 a) and the average spacing (Figure 4.16 b) between inclusions. As expected, the castings with inclusions of lower aspect ratio had higher toughness. This verifies the observation that Ca-treatment helped modifying the inclusions to a round shape, which in turn increased the toughness of the casting. As given in Equation 2 in Section 1.3, the fracture toughness varies linearly with $s^{1/2}$, where s= average inclusion spacing, and assuming the rest of the parameters to be constant. The charpy impact energy absorbed was plotted against (inclusions spacing) $^{1/2}$ and the resulting graph is linear (Figure 4.16 b), which verifies the theoretical relationship. It can be seen that the spacing between the inclusions is directly proportional to the toughness. This implies that if the inclusions are widely spaced in a sample, which means that the steel is cleaner, the toughness of the steel is increased.

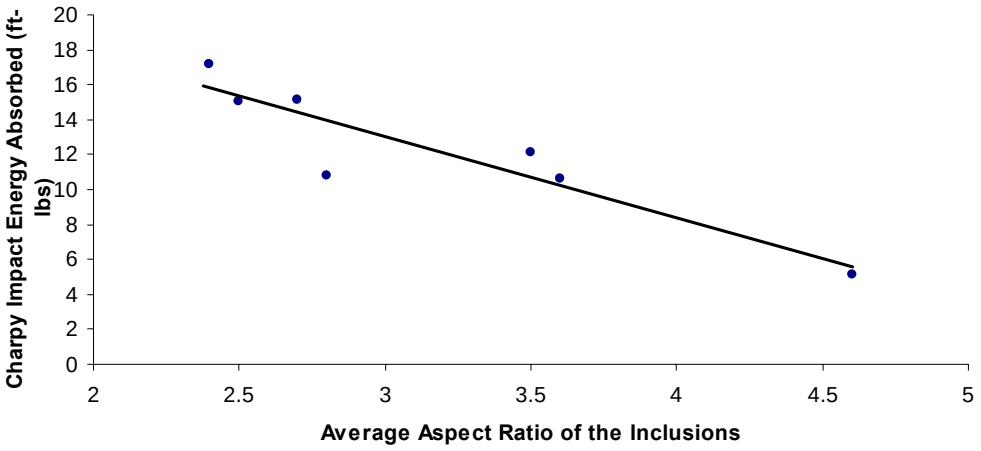

a)

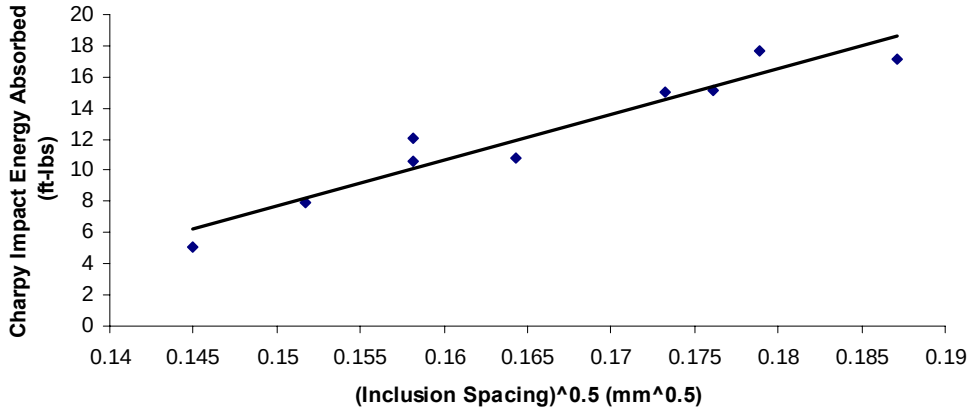

b)

Figure 4.16. Change in the charpy impact energy absorbed with change in the a) average aspect ratio of inclusion and b) (average inclusion spacing) $^{1/2}$, as measured for all the cast samples

4.3.3. Fractography. The fractured surfaces of the broken bars after the Charpy tests were observed under the Aspex SEM to determine the cause and mode of the fracture. Fractography analysis was done on two samples with highest charpy impact energy absorbed, which were, 17.2 and 16.2 ft-lbs. The mode of fracture for both the samples was found to be mostly brittle.

Figure 4.17 shows an image of a brittle crack at 500 X. The EDS analysis shows presence of alumina and manganese silicate inclusions at the crack surface, which gives a possible explanation for the brittle crack. Figure 4.18 shows presence of TiO_2-inclusions

at the brittle fracture site. The presence of these inclusions at the exact locations of the fracture further verifies that inclusions are critical to fracture toughness of steel and should be avoided.

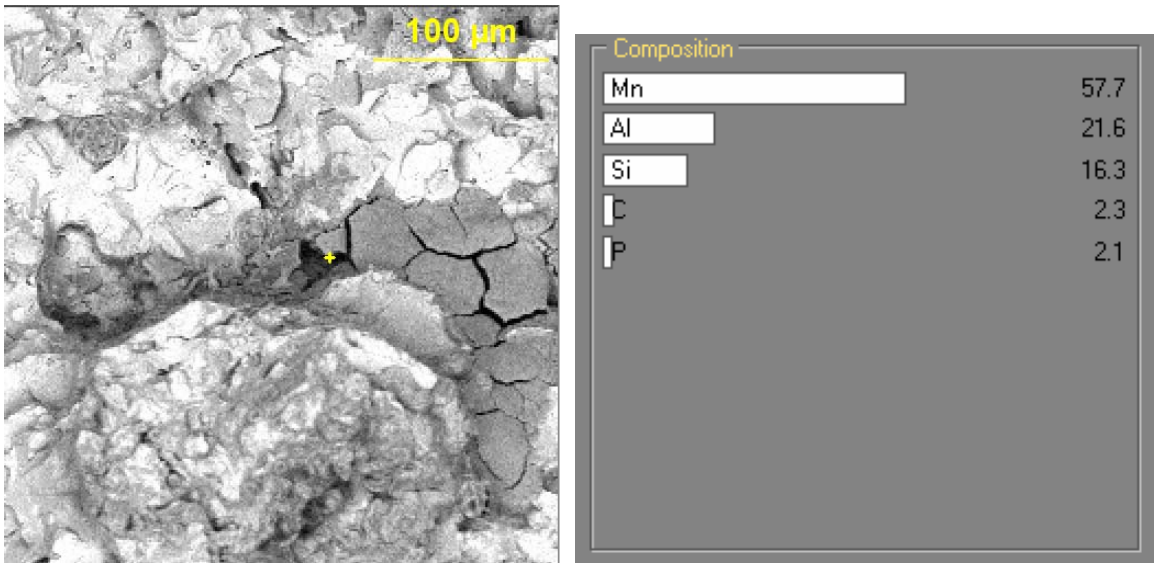

Figure 4.17. Image of a brittle fracture at 500 X obtained through Aspex, showing the presence of alumina and $MnSiO_3$ inclusions

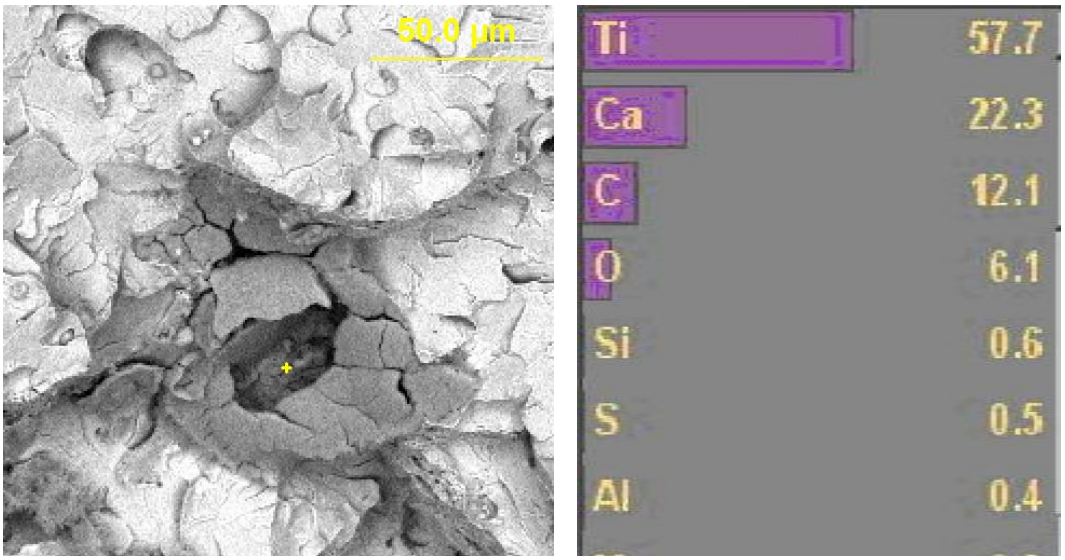

Figure 4.18. Image of a brittle fracture at 750 X obtained through Aspex, showing the presence of TiO_2 inclusions

5. CONCLUSIONS

In this research a new automated inclusion analyzer, Aspex PICA-1020, is used for identifying the number, shape, size, composition and spacing of inclusions in steel casting. The important conclusions with respect to the use of Aspex for inclusions analysis are as follows:

1) It is an integrated SEM and EDS system and allows for automated characterization of all the inclusions (1 μm to 5 mm) in a microscopic specimen; including the volume fraction, size and shape, inclusion spacing and complete inclusion identification.

2) Aspex analysis is faster than standard SEM-analysis because it only spends time collecting detailed sizing data where inclusions are known to be present, rather than spending time capturing and analyzing vast numbers of essentially empty pixels.

3) Aspex completely analyzed a standard microscopic specimen for inclusions in less than an hour.

Calcium treatment was performed in the ladle in both bulk form and wire form. Ca-addition was found to be beneficial for inclusion modification and control in the following ways:

1) In all the heats conducted with Ca-additions in the ladle, the fraction of area covered by inclusions and the total oxygen was found to decrease after the Ca-treatment.

2) The major reduction was found in alumina and MnS inclusions. The inclusions present after Ca-treatment consisted primarily of calcium aluminate and CaS inclusions.

3) The shape factor of calcium aluminate and CaS inclusions was close to 1 and their SEM images also showed their round shape, suggesting that they are not as harmful to mechanical properties of cast steel as the non-spherical inclusions.

4) The Ca-treatment trials reported a direct decrease in inclusions and total oxygen with increasing the amount of Ca-added.

5) Ca-treatment in bulk form did not cause as much decrease and modification in the inclusions as Ca-added in the form of wire.

The toughness of the cast steel was measured by conducting charpy impact tests at -40°C, after normalizing the samples. The important conclusions from the charpy tests are:

1) The charpy impact energy absorbed was found to be linearly proportional to the volume fraction of inclusions$^{-1/6}$.

2) The charpy impact energy absorbed was found to increase with an increase in the amount of Ca-added in the ladle

3) The highest toughness was obtained for the heat treated with CaSi-wire and then stirred with Ar in the ladle.

6. FUTURE WORK

Fractography analysis of the broken charpy bars can be done to analyze the mode of fracture and determine the exact cause for it. That can conclusively determine whether the void nucleation and coalescence occurring at the inclusion sites is a major source of affecting the toughness of steel. Also, charpy tests can be conducted at different temperatures to determine the ductile-to-brittle transition temperature of that steel. Instrumented Charpy tests can be done to obtain the dynamic fracture toughness, K_{1C}, which is a better representation of fracture toughness of the steel and is expected show a more direct relationship with the inclusion content.

In order to see the effect of the combination of Ar-stirring and Ca-treatment in a large ladle, samples collected from Plant C with a 20-ton ladle, will be analyzed for inclusions and total oxygen. The samples were collected before and after the Ca-treatment and the Ar-stirring in the ladle.

Ar-stirring in the ladle was beneficial for inclusion removal and produced tougher steel. Ar-stirring through a porous-plug in ladle is a better way of stirring than submerged lance-stirring. The effect of such stirring on the inclusion content and toughness of castings will be studied at Plant A.

APPENDIX A

STANDARD RULES USED FOR CLASSIFYING INCLUSIONS WITH ASPEX

Before deoxidants:

MnS Mn>30 S >20

$MnSiO_3$ Mn>20 Si>10 And S<20

MnO Mn>30 and S<20

After Al and Ti:

MnS Mn>30 S >20

$MnSiO_3$ Mn>20 Si>10 And S<20

MnO Mn>30 and S<20 and Al<25

Al_2O_3 Al>25 and Mn<25

$MnO\text{-}Al_2O_3$ Mn>25 and Al>25 and S<20

TiO_2 Ti>30

After Al, before Ca

MnS Mn>30 S >20

$MnSiO_3$ Mn>20 Si>10 And S<20

MnO Mn>30 and S<20 and Al<25

Al_2O3 Al>25 and Mn<25

$MnO\text{-}Al2O_3$ Mn>25 and Al>25 and S<20

After Ca

MnS Mn>30 S >20 and Ca<20

CaS Ca>30 S >20 and Mn<20

MnS-CaS Mn>15 and Ca>15 and S>20

$CaAl_2O_4$ Al>20 Ca>15 Si<20 Mn<20 S<20

$MnSiO_3$ Mn>20 and Si>10 and S<20 and Al<20 and Ca<20

$CaSiO_3$ Ca>20 and Si>10 and S<20 and Al<20 and Mn<20

$MnO\text{-}Al_2O_3$ Mn>25 and Al>25 and S<20 Si<20 Ca<20

CaO-MnO Ca>25 and Mn>25 and Si<20 and Al<20 and S<20

Al_2O_3 Al>25

MnO Mn>30 and S<20

CaO Ca>30 and S<20

APPENDIX B

VISUAL BASIC CODE FOR CALCULATING INCLUSION SPACING

```
Function NEAREST_NEIGHBOR(TestRange As Range, ValRange As Range)

    Dim RangeArray As Variant, TestArray As Variant
    Dim i As Long, Counter As Long
    Dim j As Integer, distance As Double, min_dist As Double
    Dim StartValRangeRow As Long, StartTestRangeRow As Long

      If ValRange.Cells.Count = 0 Then
      NEAREST_NEIGHBOR = CVErr(xlErrNum)
    Exit Function
    End If

'"Read the values into an array
    TestArray = TestRange.Value
    RangeArray = ValRange.Value

'"Identify the starting row for each argument
'"to ignore comparing a row against itself.
    StartValRangeRow = ValRange.Row
    StartTestRangeRow = TestRange.Row


'"Loop through the data and determine the minimum distance.
  For i = 1 To ValRange.Rows.Count
    If StartValRangeRow + i - 1 <> StartTestRangeRow Then
      distance = 0 ' reset distance in each pass
      Counter = Counter + 1
      For j = 1 To ValRange.Columns.Count
      distance = distance + (TestArray(1, j) - RangeArray(i, j)) ^ 2
      Next j
      If Counter = 1 Then
```

```
            min_dist = distance '"first pass must be the minimum so far
        Else
            min_dist = WorksheetFunction.Min(min_dist, distance)
        End If
    End If
    Next i

    NEAREST_NEIGHBOR = Sqr(min_dist)

End Function
```

BIBLIOGRAPHY

[1] J.W. Farrell, P.J. Bilek, D.C. Hilty, "Inclusions Originating From Reoxidation of Liquid Steel, Electric Furnace Proceedings," Vol. 28, pp. 64-88. Pittsburgh, Pennsylvania; USA; 9-11 Dec. 1970

[2] Moore and Bodor, "Steel deoxidation practice: Special emphasis on heavy section steel castings," AFS Transactions, 93, pp. 99-114, 1985

[3] R.A. Rege, E.S. Szekeres and W. D. Forgeng: Met. Trans. AIME, 1, No. 9, pp.2652, 1970

[4] R.W. Rastogi and A.W. Cramb: 2001 Steelmkaing Conf. Proc., ISS, Warrendale, PA, 2001, vol. 84, pp. 789-829

[5] L. Zhang, B.G. Thomas, "Literature Review: Inclusions in Steel Ingot Casting," Metallurgical and Materials Transactions B, Vol.37B, No.5, pp.733-761, 2006

[6] T.B. Braun, J.F. Elliott, and M.C. Flemings, Met. Trans. B, 10B, pp. 171-84, 1979

[7] T.B. Cox and J.R. Low, "Investigation of the Plastic Fracture of AISI 4340 and 18 Ni-200 Grade Maraging Steels," Met Trans A, 5A, pp.1457-1470, 1974

[8] P. Kenny and J D Campbell: Prog. Mat. Sci., 1967, 13. 135-181

[9] W.M. Garrison, "Controlling Inclusion Distributions to Achieve High Toughness in Steels," AIST Trans, 4(5), pp.132-139, 2007

[10] G.T. Hahn, M.F. Kanninen, and A.R. Rosenfield, "Annual Review of Materials Science," 2 , pp. 381-404, 1972

[11] R. Kiessling, *Non-Metallic Inclusions in Steel*, The Institute of Metals, 1989

[12] S.E. Lunner: Int. Conf. on Production and Application of Clean Steels, The Iron and Steel Institute, London, pp. 124-36, 1970

[13] H.F. Tremlett; ISI Spec. Rep. 77, 1963, London, 119-122

[14] E.T. Turkdogan, Fundamentals of steelmaking, 1996

[15] M. Herrera, F. Castro, M. Castro, M. Mendez, H. Solis, "Modification of Al2O3 inclusions in medium carbon aluminum steels by AlCaFe additions," Ironmaking and Steelmaking, 33(151), 2006

[16] M.D. Eason and R.C. Richardson, "The Effect of deoxidation practice on the quality of heavy steel castings," Technical Advances in Steel Castings; 24-25 May 1983. pp.5.1-5.7

[17] E.T. Turkdogan, Calcium Treatment Symposium, p.3. The Institute of Metals, London, 1988

[18] R.J. Fruehan, "Ladle Metallurgy Principles and Practices," ISS Warrendale PA, 1985

[19] *The Making, Shaping and Treating of Steel*, Association of Iron and Steel Engineers, 1985

[20] L.E.K. Holappa: ISS Steelmaking Conf. Proc., 83, pp. 765–777, 2001

[21] L. Holappa, M. Lind, M. Liukkonem, M. Hamalainen, "Thermodynamic examination of inclusion modification and precipitation from calcium treatment to solidified steel," Ironmaking and Steelmaking, Vol. 30, 2, pp. 111-115, 2003

[22] "Properties and Selection: Nonferrous Alloys and Special-Purpose Materials," ASM Handbook, Volume 2, 1990

[23] "An Engineering Data Book," Calvert, J. R., and Farrar, R. A., Palgrave, 1999

[24] N. Ritchie, "Automated Feature Analysis for Perception – user's document," Aspex Corporation

[25] Barbara Allyn, "Deoxidation in Heavy Section Steel Castings," Harrison Steel Castings Company, SFSA Technical and Operating Conference, 2006

[26] Ernest M. Levin, Carl. R. Robbins, Howard F. McMurdie, Phase diagrams for Ceramists, 1983

[27] Chen Chun-Li, Zhang Jin E, Li Yi-Shen "Study on an extended Boussinesq equation," Chinese Phys. 16, 2007, 2167-2179

[28] K. N. Ramakrishnan, "Modified Rosin Rammler equation for describing particle size distribution of milled powders," Journal of Materials Science Letters, Volum 9, Number 21 / November, 2000, 1903-1906

[29] S. Kimura, Y. Nabeshima, K. Nakajima, S. Mizoguchi, "Behavior of nonmetallic inclusions in front of the solid-liquid interface in low-carbon steels," Metallurgical and Materials Transactions B, Volume 31, Number 5 / October, 2000

[30] K.D.Sibley, "Effect of Si on the Impact and Tensile Properties of Low-C Steels," Metall. Trans. A, 1976 vol: 7A iss: 10, pg: 1602 -1604

[31] M. Meyers and K. Chawla, *Mechanical Behaviors of Materials*, Prentice Hall, Inc. (Pearson Education), (1999)

VITA

Vintee Singh was born on March 14, 1985. She received her primary and secondary education in India. In May of 2007, she received her Bachelor's degree in Materials and Metallurgical Engineering from Indian Institute of Technology, Kanpur, India. In December 2009, she received a Master's degree in Materials Science and Engineering from Missouri University of Science and Technology.